Safeguarding Low-Altitude Integrated Sensing and Communications Networks via UAV-Mounted RIS

Shanza Shakoor, *Student Member, IEEE,* Quang Nhat Le, *Member, IEEE,* and Trung Q. Duong, *Fellow, IEEE*

***Abstract*—In this paper, we investigate secure transmission in an integrated sensing and communication-cell-free network with the help of a low-altitude uncrewed aerial vehicle-mounted reconfigurable intelligent surface (URIS). The dual-functional access points (APs) simultaneously transmit communication signals to serve legitimate users and emit sensing signal to sense the target, who also acts as a potential eavesdropper (Eve) to intercept the communication signals. To enhance security, the artificial noise (AN) is employed by APs to degrade the Eve's reception. We formulate a sum secrecy rate maximization problem that jointly optimizes the APs' transmit beamformings, AN covariance, RIS's phase shifts, and URIS trajectory. Due to the non-convex nature of the formulated problem, it is divided into three tractable subproblems and solved by an iterative alternating optimization algorithm that incorporates the majorization–minimization framework, semidefinite relaxation, and successive convex approximation techniques. Numerical results confirm that the proposed scheme significantly improves secrecy performance compared with baseline schemes without using AN, fixed RIS, and without deploying URIS.**

***Index Terms*—Cell-free (CF), integrated sensing and communication (ISAC), physical layer security (PLS), reconfigurable intelligent surface (RIS), unmanned aerial vehicle (UAV).**

I. Introduction

The upcoming sixth-generation (6G) wireless networks are expected to deliver intelligent, high-capacity, and ultra-reliable connectivity that goes far beyond traditional communication services [1], [2]. In addition to data transmission, 6G networks are anticipated to merge communication, sensing, and computing into a unified framework that can support next-generation intelligent applications, including autonomous driving, smart manufacturing, and future smart cities [3]. Achieving this vision requires technologies capable of efficiently utilizing limited spectral and hardware resources while enabling real-time perception of the environment.

Among the key technologies envisioned for future systems, integrated sensing and communication (ISAC) has emerged as a highly promising pillar for 6G wireless networks [4]. By sharing spectrum, antennas, and hardware platforms, ISAC allows wireless nodes such as access points (APs) or base stations (BSs) to simultaneously perform information transmission and environmental sensing [5], [6]. This integration significantly enhances spectral efficiency, hardware utilization, and situational awareness, enabling wireless systems to perceive and interact with their surroundings. To further extend these advantages across wider areas, cell-free (CF)-ISAC architectures have been introduced, where multiple distributed APs cooperatively perform communication and sensing under centralized coordination [7], [8]. This distributed structure eliminates cell boundaries, mitigates interference, and provides uniform service quality with improved sensing reliability. However, the shared waveform and distributed nature of ISAC and CF systems make them inherently vulnerable to eavesdropping and information leakage [9], [10]. Because sensing and communication signals are jointly transmitted, unintended receivers or even the sensing targets themselves can intercept confidential information. These vulnerabilities have driven increasing attention towards physical layer security (PLS) techniques, which exploit the randomness of wireless channels to improve secrecy without depending solely on upper-layer cryptographic methods.

To address these challenges, recent studies have explored various PLS enhancement approaches such as artificial noise (AN) injection, secure beamforming, cooperative jamming, and joint active–passive beamforming [11]. These techniques aim to suppress the eavesdropper (Eve)'s channel while preserving the performance of legitimate users (LUs) [12]. Nevertheless, most existing PLS schemes for ISAC are limited to single-cell or static network configurations, which restrict their applicability to large-scale and dynamic 6G environments.

In parallel with terrestrial networks, low-altitude wireless networks (LAWN) have gained growing attention as a promising component of future 6G infrastructures [13]. Employing aerial platforms such as uncrewed aerial vehicles (UAVs) and low-altitude balloons, wireless networks can achieve fast deployment, adaptive coverage, and line-of-sight (LoS)-enhanced transmission, which is particularly valuable in environments with severe blockages or complex terrain [14]. Their high mobility enables real-time adjustment of network geometry, making LAWN particularly effective in emergency response, rural coverage, temporary hotspots, and sensing applications. As a result, UAV-enabled wireless systems have emerged as a valuable tool for extending network coverage and improving link quality in next-generation communication and sensing networks [15].

S. Shakoor and Q. N. Le are with the Faculty of Engineering and Applied Science, Memorial University, St. John's, NL A1C 5S7, Canada (e-mail: {sshakoor, qnle}@mun.ca).

T. Q. Duong is with the Faculty of Engineering and Applied Science, Memorial University, St. John's, NL A1C 5S7, Canada, and is also with the School of Electronics, Electrical Engineering and Computer Science, Queen's University Belfast, Belfast, U.K. (e-mail: tduong@mun.ca).

This paper has been submitted in part for presentation at the International Conference on Synergies in Next-Generation Cyber-Physical Systems (SNGC 2026), Cardiff, UK, September 2026.

This work was supported in part by the Canada Excellence Research Chair (CERC) Program CERC-2022-00109 and in part by the Natural Sciences and Engineering Research Council of Canada (NSERC) Discovery Grant Program RGPIN-2025-04941.

Motivated by these capabilities, researchers have begun integrating UAVs with reconfigurable intelligent surfaces (RISs) to further enhance wireless propagation [16]. A passive RIS, composed of tunable reflecting elements, can intelligently reconfigure its phase shifts to steer signals toward legitimate receivers and away from potential Eves, thereby strengthening both secure communication and sensing accuracy. When mounted on a UAV, the RIS gains three-dimensional (3D) mobility, enabling dynamic positioning to maintain favorable LoS links and extend network coverage [17]. The combination of UAV mobility, RIS reconfigurability, and CF cooperation creates new opportunities for secure and adaptive ISAC design. However, the PLS of UAV-mounted RIS (URIS) assisted CF-ISAC systems remains largely unexplored, particularly when the sensing target acts as a potential Eve.

To fill this gap, this paper develops a comprehensive URIS-assisted CF-ISAC framework with an emphasis on PLS enhancement. The URIS provides flexible control of reflected propagation paths by adjusting its 3D position and phase shifts, enabling stronger links for LUs while suppressing eavesdropping. To maximize the secrecy rate, we jointly optimize AN, active beamforming, passive RIS reflection, and URIS location. The resulting optimization problem is inherently non-convex and is addressed using an efficient successive convex approximation (SCA)-based alternating optimization (AO) algorithm.

A. Related Work

Security in ISAC systems has become an important research topic due to the dual use of the transmitted waveform for both data communication and sensing. Several studies have examined PLS through AN, secure beamforming, and robust optimization [18], [19]. The work in [20] analyzed joint sensing, communication, and security, and introduced AN-aided signaling to reduce information leakage. The authors in [10] designed a secure ISAC beamforming framework that enhanced sensing accuracy while controlling the Eve's received power. In [21], the sensing target was treated as a potential Eve, and the signal-to-noise-ratio (SNR) at the target was intentionally reduced through the joint optimization of AN and dual-functional beamforming. Robust ISAC security considering imperfect channel state information (CSI) and multiple suspicious targets was explored in [22]. While these studies demonstrate the importance of securing ISAC signaling, they mainly focus on single-cell architectures with fixed terrestrial deployments and do not incorporate distributed APs, cooperative processing, or low-altitude aerial platforms.

Research on CF massive multi-input–multi-output (MIMO) has shown that distributed APs can provide uniform service quality, interference suppression, and improved robustness. The study in [23] analyzed secrecy performance in CF systems through optimized AP selection and user grouping. The authors in [24] investigated ISAC in CF architectures and demonstrated that coordinated AP processing can enhance both sensing and communication performance. In [25], secrecy was strengthened through AP power allocation, while [26] developed an AP association strategy to suppress information leakage.

LAWN, supported by UAVs, have been widely studied for enabling reliable communication and sensing in environments characterized by blockage, shadowing, or dynamic channel conditions [14]. UAV mobility allows the network to maintain favorable LoS links by adjusting altitude and horizontal position. Within this context, URIS offer a passive and energy-efficient approach for shaping propagation. The work in [27] considered URIS placement to enhance reflected signal paths, and the study in [28] investigated RIS phase configuration to improve joint communication and sensing performance. By selecting the UAV's 3D position and configuring RIS's phase shifts, URIS can direct reflected signals towards desired users or sensing targets and provide LoS opportunities that complement distributed APs. Existing URIS studies primarily address coverage improvement, reflection control, or rate enhancement, they do not examine PLS within CF-ISAC networks.

In summary, although ISAC security, CF cooperation, and URIS-assisted propagation control have each been investigated independently, the joint integration of these three technologies has not been explored. To the best of our knowledge, no existing work considers a URIS-assisted CF-ISAC framework designed explicitly for PLS, which forms the central contribution of this paper.

B. Motivation and Contributions

The integration of sensing and communication in CF-ISAC networks significantly increases the risk of confidential information leakage, as the dual-functional waveform may be intercepted not only by unintended users but also by the sensing target itself [10], [20]. Unlike traditional cellular ISAC architectures, the spatially distributed nature of CF networks broadens the exposure region of transmitted signals, making secure waveform design more challenging and highly dependent on the underlying spatial channel characteristics and electromagnetic scattering environment [7], [23]. RISs have emerged as an effective technology for passive propagation manipulation, enabling energy-efficient spatial control to enhance legitimate links and suppress Eves [16], [28]. Meanwhile, low-altitude UAV platforms provide dynamic 3D mobility, allowing flexible placement and robust LoS connectivity even in highly obstructed or non-LoS (NLoS)-dominated propagation environments [13], [14], [29]. The combination of UAV mobility with RIS reconfigurability in a URIS architecture unlocks additional spatial degrees of freedom that cannot be achieved with static RIS or terrestrial-only ISAC deployments.

Despite these advantages, secure low-altitude URIS-assisted CF-ISAC design remains largely unexplored, especially for scenarios in which the sensing target also acts as a potential Eve, a security threat that is intrinsic to ISAC signaling that has not been adequately addressed in existing literature. To the best of our knowledge, no prior work has jointly optimized APs' transmit beamformings, AN, RIS's phase shifts, and URIS trajectory for PLS in CF-ISAC networks, which constitutes the core motivation for this work.

The main contributions of this work are summarized as follows:

- We propose a CF-ISAC architecture where a RIS is mounted on a UAV to enhance both radar sensing and secure downlink communication. The URIS dynamically adjusts its horizontal trajectory and phase shifts to strengthen legitimate links while degrading eavesdropping channels.
- We develop a sum secrecy rate maximization framework that performs a joint optimization of the APs' transmit beamforming vectors, AN covariance, RIS's phase shifts, and the URIS trajectory subject to communication, sensing, and mobility constraints.
- To address the inherent non-convexity of the formulated problem, we design an AO algorithm leveraging majorization-minimization (MM), semidefinite relaxation (SDR), and SCA.
- We compare the proposed framework against three baseline schemes: (i) without AN, (ii) fixed RIS (no UAV mobility), and (iii) without URIS. Simulation results show that the proposed scheme achieves significant sum secrecy rate improvement due to the combined benefits of using AN, URIS passive beamforming, and UAV mobility.

C. Paper Organization and Notations

Section II describes the secure low-altitude URIS-assisted CF-ISAC system model. Section III develops the sum secrecy rate maximization problem. Section IV describes the proposed AO algorithm. Section V present simulation results and performance comparisons. Finally, section VI concludes the paper. For ease, a summary of the key notations used throughout the paper is provided in Table I.

Notations: We denote vectors by bold lowercase (e.g., $\mathbf{w}$) and matrices by bold uppercase (e.g., $\mathbf{W}$). The transpose, conjugate, and conjugate transpose (Hermitian transpose) of $\mathbf{W}$ are written as $\mathbf{W}^T$, $\mathbf{W}^\dagger$, and $\mathbf{W}^H$, respectively. The absolute value and Euclidean norm of $\mathbf{W}$ are denoted by $|\mathbf{W}|$ and $\|\mathbf{W}\|$, respectively. The space of $M \times 1$ complex-valued vectors and $M \times N$ complex-valued matrices are represented by $\mathbb{C}^{M\times 1}$ and $\mathbb{C}^{M\times N}$, respectively. $\mathrm{diag}(\boldsymbol{\theta})$ forms a diagonal matrix with elements of $\boldsymbol{\theta}$, $\Re\{\cdot\}$ extracts the real part, and $\mathbf{I}_N$ denotes the $N \times N$ identity matrix.

TABLE I
VARIABLE DEFINITION

Notation	Description
L	Number of APs
K	Number of LUs
M	Number of antennas at each AP
N	Number of reflecting elements at each RIS
T	Total number of time slots
t	Time slot index
$\mathbf{q}(t)$	3D position vector of URIS at time slot t
$\mathbf{w}_{0,l}(t)$	Beamforming vector of AP l at time slot t for potential target
$\mathbf{w}_{k,l}(t)$	Beamforming vector of AP l at time slot t for LU k
$\mathbf{W}_l(t)$	Combined beamforming matrix of AP l
$\mathbf{v}_l(t)$	AN vector at time slot t
$\boldsymbol{\Theta}(t)$	Diagonal phase-shift matrix of RIS at time slot t
$\mathbf{d}_{l,q}(t)$	Distance between AP l and URIS at time slot t
$\mathbf{d}_{q,e}(t)$	Distance between URIS and target at time slot t
$\mathbf{d}_{q,k}(t)$	Distance between URIS and LU k at time slot t
$\mathbf{H}_{l,q}(t)$	Channel from AP l to URIS at time slot t
$\mathbf{h}_{k,l}(t)$	Direct channel vector from AP l to LU k at time slot t
$\mathbf{h}_{q,k}(t)$	Channel from URIS to LU k at time slot t
$\mathbf{h}_{q,e}(t)$	Channel from URIS to target at time slot t
$\mathbf{h}_{e,l}^{\mathrm{URIS}}(t)$	Cascaded channel AP-URIS-target/Eve at time slot t
$\mathbf{h}_{k,l}^{\mathrm{URIS}}(t)$	Cascaded channel AP-URIS-LU at time slot t
$\mathbf{h}_{k,l}^{H}(t)$	Effective propagation channels from the AP l to the LU k at time slot t
$\mathbf{h}_{e,l}^{H}(t)$	Effective propagation channels from the AP l to the Eve at time slot t
$\gamma_s(t)$	Joint sensing SNR
$\mathbf{R}_k(t)$	Sum rate of all LUs at time slot t

II. System Model

As illustrated in Fig. 1, we consider a CF-ISAC system assisted by a single URIS. The system comprises a set of geographically distributed APs, denoted by $\mathcal{L} = \{1, 2, \ldots, L\}$, where each AP utilizes a uniform linear array (ULA) consisting of M transmit/receive antennas, arranged with a half-wavelength spacing of $\lambda/2$, where λ denotes the carrier wavelength. The system serves a set of LUs $\mathcal{K} = \{1, 2, \ldots, K\}$, each equipped with a single antenna, along with a potential target, which may act as an Eve attempting to intercept LUs communication. The APs transmit dual-functional radar-communication (DFRC) signals, enabling simultaneous downlink communication with the users and probing of the target for radar sensing. Additionally, AN can be transmitted from the APs to enhance secure communication by degrading the Eve channel quality. A single URIS is deployed to assist the system. It is equipped with a set of passive reflecting elements $\mathcal{N} = \{1, 2, \ldots, N\}$, each capable of independently adjusting its phase shift to intelligently reconfigure the wireless propagation environment. A central processing unit (CPU) coordinates the APs and the URIS through reliable wired or wireless backhaul links that are assumed to introduce no transmission errors.

A single URIS is deployed to assist the system. The URIS operates within a predefined 3D flight region

$$\mathcal{Q} = \{(x, y, H) \mid x_{\min} \le x \le x_{\max},\ y_{\min} \le y \le y_{\max}\},$$

where H denotes its fixed operating altitude. The UAV dynamics are subject to a maximum horizontal displacement

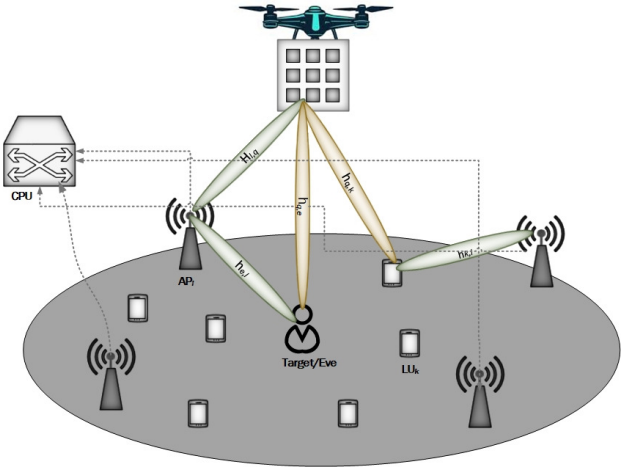

Fig. 1. Secure Low-Altitude URIS-aided CF-ISAC System Model.

per time slot, which reflects its velocity constraint:

$$\|\mathbf{q}[t+1]-\mathbf{q}[t]\| \le v_{\max}\varrho_t, \qquad t=1,\dots,T-1,$$

where $\mathbf{q}[t]$ is the UAV horizontal coordinate at time slot t, $v_{\max}$ is the maximum UAV speed, and ϱ_t is the slot duration. These mobility restrictions ensure physically realizable URIS motion and enable trajectory optimization to exploit favorable sensing and communication geometries.

A. Signal Transmission Model

At each time slot, the transmitted signal at the l-th AP consists of three components: (i) information signals for the LUs, (ii) a radar probing signal for target detection, and (iii) AN to enhance PLS.

Let $s_k(t) \sim \mathcal{CN}(0,1)$ denote the information symbol for user $k \in \mathcal{K}$ and $s_0(t) \sim \mathcal{CN}(0,1)$ denote the radar probing symbol. For notational consistency, the overall symbol vector can be defined as

$$\mathbf{s}(t) = \begin{bmatrix} s_0(t) \\ s_1(t) \\ \vdots \\ s_K(t) \end{bmatrix} \in \mathbb{C}^{(K+1)\times 1}, \tag{1}$$

such that

$$\mathbb{E}\{\mathbf{s}(t)\mathbf{s}(t)^H\} = \mathbf{I}_{(K+1)}. \tag{2}$$

The local beamforming vectors at the l-th AP are denoted by $\mathbf{w}_{0,l}(t) \in \mathbb{C}^{M\times 1}$ for the radar and $\mathbf{w}_{k,l}(t) \in \mathbb{C}^{M\times 1}$ for LU k. Let $\mathbf{v}_l(t) \in \mathbb{C}^{M\times 1}$ denote the AN vector at the l-th AP. For the l-th AP, the combined beamforming matrix is expressed as

$$\mathbf{W}_l(t) = \left[\mathbf{w}_{0,l}(t),\ \mathbf{w}_{1,l}(t),\ \dots,\ \mathbf{w}_{K,l}(t)\right] \in \mathbb{C}^{M\times(K+1)}. \tag{3}$$

Then, the transmit signal at the l-th AP in time slot t can be written as

$$\begin{aligned}\mathbf{x}_l(t) &= \sum_{k\in\tilde{\mathcal{K}}} \mathbf{w}_{k,l}(t)\, s_k(t) + \mathbf{v}_l(t) \\ &= \mathbf{W}_l(t)\,\mathbf{s}(t) + \mathbf{v}_l(t),\end{aligned} \tag{4}$$

where $\tilde{\mathcal{K}} \triangleq \{0\} \cup \mathcal{K}$ (index 0 denotes the sensing target).

B. Channel Model

We adopt a quasi-static block fading assumption in which the channels remain unchanged within each transmission block and vary across blocks due to UAV movement. Let the URIS be deployed at altitude H with horizontal position $\mathbf{p}_q(t) = [x_q(t), y_q(t)]^\top$, such that its 3D position is $\mathbf{q}(t) = [x_q(t), y_q(t), H]^\top$. Each AP $l \in \mathcal{L}$ is located at $\mathbf{p}_l = [x_l, y_l, 0]^\top$, LU $k \in \mathcal{K}$ is at $\mathbf{p}_k = [x_k, y_k, 0]^\top$, and the potential target/Eve is at $\mathbf{p}_e = [x_e, y_e, 0]^\top$.

1) AP→URIS Channel: The distance between AP l and the URIS is

$$d_{l,q}(t) = \sqrt{\|\mathbf{q}(t) - \mathbf{p}_l\|^2}. \tag{5}$$

Ignoring atmospheric scattering, the AP→URIS channel is dominated by the LoS component when H is sufficiently large. The channel matrix from AP l to URIS can thus be expressed as

$$\mathbf{H}_{l,q}(t) = \sqrt{J_0 d_{l,q}(t)^{-\alpha_1}}\, \tilde{\mathbf{H}}_{l,q}(t), \tag{6}$$

where J_0 is the reference path gain at 1 m, α_1 is the air-to-ground pathloss exponent, and $\tilde{\mathbf{H}}_{l,q}(t) \in \mathbb{C}^{N\times M}$ can be given by

$$\mathbf{H}_{l,q}(t) = \mathbf{a}_q(\zeta_{l,q}(t)) \otimes \mathbf{a}_l(\xi_{l,q}(t)), \tag{7}$$

where $\mathbf{a}_q(\cdot) \in \mathbb{C}^{N\times 1}$ is the URIS array response vector defined as

$$\mathbf{a}_q(\zeta_{l,q}) = \left[1, e^{-j\frac{2\pi d_q \cos(\zeta_{l,q})}{\lambda}}, \dots, e^{-j\frac{2\pi d_q (N-1)\cos(\zeta_{l,q})}{\lambda}}\right]^H, \tag{8}$$

and $\mathbf{a}_l(\cdot) \in \mathbb{C}^{M\times 1}$ is the transmit array response vector at the l-th AP expressed as

$$\mathbf{a}_l(\xi_{l,q}) = \left[1, e^{-j\frac{2\pi d_l}{\lambda}\sin(\xi_{l,q})}, \dots, e^{-j\frac{2\pi d_l}{\lambda}(M-1)\sin(\xi_{l,q})}\right], \tag{9}$$

where d_q and d_l denote the inter-element spacings at the URIS and AP, respectively, and λ denotes the carrier wavelength. Here, $\zeta_{\ell,q}(t), \xi_{\ell,q}(t)$ correspond to the elevation angle of arrival (AoA) and azimuth angle of departure (AoD), respectively, with $\cos(\zeta_{l,q}) = |x_l - x_q|/d_{l,q}$ and $\sin(\xi) = |y_l - y_q|/d_{l,q}$.

2) URIS→LU/Target/Eve Channels: The distance from the URIS to LU k is

$$d_{q,k}(t) = \sqrt{\|\mathbf{q}(t) - \mathbf{p}_k\|^2}, \tag{10}$$

and the URIS→LU k channel is given by

$$\mathbf{h}_{q,k}(t) = \sqrt{J_0 d_{q,k}(t)^{-\alpha_1}}\, \tilde{\mathbf{h}}_{q,k}(t), \tag{11}$$

where $d_{g,k}(t)$ denotes the distance between the URIS and LU k, and $\mathbf{h}_{q,k}(t)$ can be expressed as

$$\tilde{\mathbf{h}}_{q,k}(t) = \left[1, e^{-j\frac{2\pi d_{q,k}\cos(\varphi_{q,k})}{\lambda}}, \ldots, e^{-j\frac{2\pi d_{q,k}(N-1)\cos(\varphi_{q,k})}{\lambda}}\right]^H, \tag{12}$$

where $\cos(\varphi_{q,k}) = |x_q - x_k|/d_{q,k}$. Similarly, the URIS→target/Eve channel is given by

$$\mathbf{h}_{q,e}(t) = \sqrt{J_0 d_{q,e}(t)^{-\alpha_1}}\,\tilde{\mathbf{h}}_{q,e}(t), \tag{13}$$

where $d_{q,e}(t) = \sqrt{\|\mathbf{q}(t) - \mathbf{p}_e\|^2}$ and $\tilde{\mathbf{h}}_{q,e}(t)$ can be given by

$$\tilde{\mathbf{h}}_{q,e}(t) = \left[1, e^{-j\frac{2\pi d_{q,e}\cos(\varphi_{q,e})}{\lambda}}, \ldots, e^{-j\frac{2\pi d_{q,e}(N-1)\cos(\varphi_{q,e})}{\lambda}}\right]^H. \tag{14}$$

3) Direct AP→LU/Target/Eve Channels: Due to ground scattering, the AP→LU and AP→target links are modeled by Rician fading. The direct channel from AP ℓ to LU k is

$$\begin{aligned}\mathbf{h}_{k,l} &= \sqrt{J_0 d_{k,l}^{-\alpha_2}}\left(\sqrt{\frac{\kappa_{k,l}}{\kappa_{k,l}+1}}\,\mathbf{h}_{k,l}^{\text{LoS}} + \sqrt{\frac{1}{\kappa_{k,l}+1}}\,\mathbf{h}_{k,l}^{\text{NLoS}}\right),\\ &= \sqrt{J_0 d_{k,l}^{-\alpha_2}}\tilde{\mathbf{h}}_{k,l},\end{aligned} \tag{15}$$

where $d_{k,l} = \|\mathbf{p}_l - \mathbf{p}_k\|$, α_2 is the ground pathloss exponent, $\kappa_{k,l}$ is the distance-dependent Rician factor, $\mathbf{h}_{k,l}^{\text{LoS}}$ is the deterministic LoS steering vector, and $\mathbf{h}_{k,l}^{\text{NLoS}} \sim \mathcal{CN}(\mathbf{0}, \mathbf{I}_M)$ is the NLoS component. The direct AP→target/Eve channel is modeled as

$$\begin{aligned}\mathbf{h}_{e,l} &= \sqrt{J_0 d_{l,e}^{-\alpha_2}}\left(\sqrt{\frac{\kappa_{l,e}}{\kappa_{l,e}+1}}\,\mathbf{h}_{l,e}^{\text{LoS}} + \sqrt{\frac{1}{\kappa_{l,e}+1}}\,\mathbf{h}_{l,e}^{\text{NLoS}}\right),\\ &= \sqrt{J_0 d_{e,l}^{-\alpha_2}}\tilde{\mathbf{h}}_{e,l},\end{aligned} \tag{16}$$

where $\mathbf{h}_{l,e}^{\text{NLoS}} \sim \mathcal{CN}(\mathbf{0}, \mathbf{I}_M)$ represents the scattering vector.

4) Effective Channels: We denote $\mathbf{h}_{k,l} \in \mathbb{C}^{M\times 1}$ and $\mathbf{h}_{e,l} \in \mathbb{C}^{M\times 1}$ as the direct channels from the l-th AP to the k-th LU and to the Eve, respectively. The cascaded AP→URIS→LU and AP→URIS→target/Eve channel is expressed as

$$\begin{aligned}\mathbf{h}_{k,l}^{\text{URIS}}(t) &= \mathbf{h}_{q,k}^H(t)\boldsymbol{\Theta}(t)\mathbf{H}_{l,q}(t)\\ &= \boldsymbol{\theta}^T(t)\text{diag}(\mathbf{h}_{q,k}^H(t))\mathbf{H}_{l,q}(t)\\ &= \boldsymbol{\theta}^T(t)\mathbf{G}_{k,q}(t),\end{aligned} \tag{17}$$

$$\begin{aligned}\mathbf{h}_{e,l}^{\text{URIS}}(t) &= \mathbf{h}_{q,e}^H(t)\boldsymbol{\Theta}(t)\mathbf{H}_{l,q}(t)\\ &= \boldsymbol{\theta}^T(t)\text{diag}(\mathbf{h}_{q,e}^H(t))\mathbf{H}_{l,q}(t)\\ &= \boldsymbol{\theta}^T(t)\mathbf{G}_{e,q}(t),\end{aligned} \tag{18}$$

where $\boldsymbol{\Theta}(t) = \text{diag}(e^{j\varphi_1(t)}, \ldots, e^{j\varphi_N(t)}) = \text{diag}(\theta_1(t), \ldots, \theta_N(t))$, $\boldsymbol{\theta}(t) = [\theta_1(t), \ldots, \theta_N(t)]^T$ with $|\theta_n| = 1, \forall n \in \mathcal{N}$, represents the URIS reflection matrix. The effective propagation channels from the l-th AP to the k-th LU and to the Eve are respectively defined as

$$\hat{\mathbf{h}}_{k,l}^H(t) = \mathbf{h}_{k,l}^H + \mathbf{h}_{k,l}^{\text{URIS}}(t). \tag{19}$$

$$\hat{\mathbf{h}}_{e,l}^H(t) = \mathbf{h}_{e,l}^H + \mathbf{h}_{e,l}^{\text{URIS}}(t). \tag{20}$$

C. Communication Model

The received baseband signal at the k-th LU in time slot t can be expressed as

$$y_k(t) = \sum_{l\in\mathcal{L}} \hat{\mathbf{h}}_{k,l}^H(t)\mathbf{x}_l(t) + n_k(t). \tag{21}$$

Based on (21), the received signal-to-interference-plus-noise ratio (SINR) at the k-th LU is expressed as

$$\gamma_k(t) = \frac{\left|\sum_{l\in\mathcal{L}} \hat{\mathbf{h}}_{k,l}^H(t)\mathbf{w}_{k,l}(t)\right|^2}{\sum_{j\in\tilde{\mathcal{K}}\setminus k}\left|\sum_{l\in\mathcal{L}} \hat{\mathbf{h}}_{k,l}^H(t)\mathbf{w}_{j,l}(t)\right|^2 + \left|\sum_{l\in\mathcal{L}} \hat{\mathbf{h}}_{k,l}^H(t)\mathbf{v}_l(t)\right|^2 + \sigma_k^2}. \tag{22}$$

The achievable rate of the k-th LU is defined as

$$R_k(t) = \log_2\left(1 + \gamma_k(t)\right). \tag{23}$$

D. Security Model

The received signal at the target/Eve during time slot t is expressed as

$$y_e(t) = \sum_{l\in\mathcal{L}}\left(\mathbf{h}_{e,l}^H + \mathbf{h}_{q,e}^H(t)\boldsymbol{\Theta}(t)\mathbf{H}_{l,q}(t)\right)\mathbf{x}_l(t) + n_e(t), \tag{24}$$

where $n_e(t) \sim \mathcal{CN}(0, \sigma_e^2)$ is AWGN at the target/Eve. Accordingly, the SINR at the target/Eve for intercepting the k-th LU's stream is given by [9]

$$\gamma_{e,k}(t) = \frac{\left|\sum_{l\in\mathcal{L}} \hat{\mathbf{h}}_{e,l}^H(t)\mathbf{w}_{k,l}(t)\right|^2}{\sum_{j\in\tilde{\mathcal{K}}\setminus\{k\}}\left|\sum_{l\in\mathcal{L}} \hat{\mathbf{h}}_{e,l}^H(t)\mathbf{w}_{j,l}(t)\right|^2 + \left|\sum_{l\in\mathcal{L}} \hat{\mathbf{h}}_{e,l}^H(t)\mathbf{v}_l\right|^2 + \sigma_e^2}. \tag{25}$$

Accordingly, the achievable secrecy rate of LU k is then expressed as

$$R_k^{\text{Sec}}(t) = \left[R_k(t) - R_{e,k}(t)\right]^+, \tag{26}$$

where $R_{e,k}(t) = \log_2(1 + \gamma_{e,k}(t))$ and $[x]^+ = \max(0, x)$.

E. Sensing Model

The radar signal received by l-th AP during time slot t can be expressed as [30]

$$
\begin{aligned}
y_{e,l}(t) &= \sum_{\acute{l}\in\mathcal{L}} \alpha_{\acute{l}}^{l}\, \hat{\mathbf{h}}_{e,l}(t)\hat{\mathbf{h}}_{e,\acute{l}}^{H}(t)\, \mathbf{x}_{\acute{l}}(t) + \mathbf{n}_l(t) \\
&= \sum_{\acute{l}\in\mathcal{L}} \alpha_{\acute{l}}^{l}\, \hat{\mathbf{h}}_{e,l}(t)\hat{\mathbf{h}}_{e,\acute{l}}^{H}(t) \big[\mathbf{W}_{\acute{l}}(t)\mathbf{s}(t) + \mathbf{v}_{\acute{l}}(t)\big] + \mathbf{n}_l(t) \\
&= \sum_{\acute{l}\in\mathcal{L}} \alpha_{\acute{l}}^{l}\, \hat{\mathbf{h}}_{e,l}(t)\hat{\mathbf{h}}_{e,\acute{l}}^{H}(t)\, \mathbf{W}_{\acute{l}}(t)\mathbf{s}(t) \\
&+ \sum_{\acute{l}\in\mathcal{L}} \alpha_{\acute{l}}^{l}\, \hat{\mathbf{h}}_{e,l}(t)\hat{\mathbf{h}}_{e,\acute{l}}^{H}(t)\, \mathbf{v}_{\acute{l}}(t) + \mathbf{n}_l(t),
\end{aligned} \tag{27}
$$

where $\alpha_{\acute{l}}^{l}$ represents the radar cross section (RCS) of the target from the transmitting AP l to the receiving AP $\acute{l}$. According to the Swerling-I model, the RCS is assumed to remain constant throughout the transmission period and is modeled as a complex Gaussian random variable $\alpha_{\acute{l}}^{l} \sim \mathcal{CN}(\mathbf{0}, (\sigma_{\acute{l}}^{l})^2)$. The receiver noise at the l-th AP is denoted by

$$
\mathbf{n}_l(t) \sim \mathcal{CN}(\mathbf{0}, \sigma_l^2 \mathbf{I}_M). \tag{28}
$$

Hence, the joint sensing SNR at the CPU can be derived by jointly processing the signals from all APs, which is given by

$$
\gamma_s(t) = \frac{\sum\limits_{l\in\mathcal{L}} (\sigma_{\acute{l}}^{l})^2 \big|\big| \sum\limits_{\acute{l}\in\mathcal{L}} \mathbf{H}_{e,l,\acute{l}}(t)\mathbf{W}_{\acute{l}}(t) \big|\big|^2}{\sum\limits_{l\in\mathcal{L}} \big|\big| \sum\limits_{\acute{l}\in\mathcal{L}} \mathbf{H}_{e,l,\acute{l}}(t)\mathbf{v}_{\acute{l}}(t) \big|\big|^2 + \sum\limits_{l\in\mathcal{L}} \sigma_l^2}, \tag{29}
$$

where $\mathbf{H}_{e,l,\acute{l}}(t) \triangleq \hat{\mathbf{h}}_{e,l}(t)\hat{\mathbf{h}}_{e,\acute{l}}^{H}(t)$. The joint sensing SNR in (29) is obtained after centralized fusion at the CPU. Specifically, each AP forwards its received sensing signal to the CPU, which performs coherent joint processing across all APs. By phase-aligning and combining the received echoes, the CPU exploits spatial diversity and accumulates the reflected signal power constructively.

III. Problem Formulation

Our objective is to maximize the sum secrecy rate of all LUs through a joint optimization of the APs' transmit beamforming $\mathbf{w}(t) \triangleq \{\mathbf{w}_{k,l}(t)\}_{k\in K, l\in L}$, the URIS reflection vector $\boldsymbol{\theta}(t)$, the covariance of the AN vectors $\mathbf{R}_v(t) \triangleq \{\mathbf{R}_l(t)\}_{l\in L}$, where $\mathbf{R}_l(t) \triangleq \mathbf{v}_l(t)\mathbf{v}_l^H(t)$, and the URIS deployment location $\mathbf{q}(t)$. Accordingly, the optimization problem is given by

$$
\max_{\substack{\mathbf{w}(t),\boldsymbol{\theta}(t),\\ \mathbf{R}_v(t),\mathbf{q}(t),\forall t}} \sum_{t\in T}\sum_{k\in\mathcal{K}} R_k^{\text{Sec}}(t) \tag{30a}
$$

s.t.

$$
\sum_{k\in\mathcal{K}} ||\mathbf{w}_{k,l}(t)||^2 + \text{Tr}(\mathbf{R}_l(t)) \le P_l^{\max}, \quad \forall l, \forall t, \tag{30b}
$$

$$
\gamma_s(t) \ge \gamma_s^{\min}, \forall t, \tag{30c}
$$

$$
R_k^{\text{Sec}}(t) \ge R_k^{\min}, \quad \forall k,\ \forall t, \tag{30d}
$$

$$
|\theta_n(t)| = 1, \forall n, \forall t, \tag{30e}
$$

$$
\mathbf{R}_l(t) = \mathbf{R}_l(t)^H, \mathbf{R}_l(t) \ge 0, \forall l, \forall t, \tag{30f}
$$

$$
\mathbf{q}(t) \in \mathcal{Q}, \forall t, \tag{30g}
$$

$$
\frac{||\mathbf{q}(t) - \mathbf{q}(t-1)||}{\varrho} \le v_{max}, \forall t, \tag{30h}
$$

where constraint (30b) limits the maximum transmit power of the l-th AP, i.e., $P_l^{\max}$. Constraint (30c) ensures the minimum sensing SNR requirement γ_s^{min}. Constraint (30d) maintains LU quality of service (QoS). The unit-modulus condition of URIS elements is given by the constraint (30e). Constraint (30f) ensures the AN covariance matrix is Hermitian and positive semidefinite. Constraints (30g) and (30h) define the UAV's feasible region and velocity limits.

IV. Proposed Solution

In this section, we propose an AO framework to solve problem (30) by decomposing it into three sub-problems, which are updated sequentially. In each iteration, one variable among $\mathbf{w}(t)$, $\boldsymbol{\theta}(t)$, $\mathbf{R}_v(t)$, and $\mathbf{q}(t)$ is optimized while keeping the others fixed, and the process repeats until convergence. To enable efficient computation, the objective function and non-convex constraints are reformulated, and each sub-problem is solved using MM, SDR, and SCA techniques. This AO framework facilitates joint optimization of $\mathbf{w}(t)$, $\boldsymbol{\theta}(t)$, $\mathbf{R}_v(t)$, and $\mathbf{q}(t)$ in a computationally tractable manner.

A. Transmit Beamforming and AN Optimization

With fixed $\boldsymbol{\theta}(t)$ and $\mathbf{q}(t)$, the problem (30) reduces to a subproblem for optimizing $\mathbf{w}(t)$ and $\mathbf{R}_v(t)$, which is formulated as

$$
\max_{\substack{\mathbf{w}(t),\\ \mathbf{R}_v(t),\forall t}} \sum_{t\in T}\sum_{k\in\mathcal{K}} R_k^{\text{Sec}}(t) \tag{31a}
$$

s.t.

$$
\text{(30b), (30c), (30d), (30f).} \tag{31b}
$$

Problem (31) is non-convex because the objective function in (31a) is not concave and constraints (30c) and (30d) are non-convex. Let us define $\mathbf{H}_{i,l,\acute{l}}(t) = \hat{\mathbf{h}}_{i,l}(t)\hat{\mathbf{h}}_{i,\acute{l}}^{H}(t)$ and $\mathbf{W}_{i,l}(t) = \mathbf{w}_{i,l}(t)\mathbf{w}_{i,l}^{H}(t)$, for $i \in \{k, e\}$. The optimization problem to be equivalently rewritten as

$$\max_{\substack{\mathbf{W}_{k,l}(t),\mathbf{R}_v(t),\\ \forall k,\forall l,\forall t}} \sum_{t\in T}\sum_{k\in\mathcal{K}} \quad R_k^{\text{Sec}}(t) \tag{32a}$$

s.t.

$$\sum_{k\in\mathcal{K}} \text{Tr}(\mathbf{W}_{k,l}(t)) + \text{Tr}(\mathbf{R}_l(t)) \le P_l^{\max}, \quad \forall l,\forall t, \tag{32b}$$

$$\sum_{l\in\mathcal{L}}(\sigma_{\acute{l}}^l)^2 \sum_{k\in\tilde{\mathcal{K}}} \text{Tr}\Big(\sum_{\acute{l}\in\mathcal{L}} \mathbf{H}_{e,l,\acute{l}}(t)\mathbf{W}_{k,l}(t)\mathbf{H}_{e,l,\acute{l}}^H(t)\Big)$$
$$- \gamma_s^{\min}\sum_{l\in\mathcal{L}} \text{Tr}\Big(\sum_{\acute{l}\in\mathcal{L}} \mathbf{H}_{e,l,\acute{l}}(t)\mathbf{R}_{\acute{l}}(t)\mathbf{H}_{e,l,\acute{l}}^H(t)\Big)$$
$$- \gamma_s^{\min}\sum_{l\in\mathcal{L}}\sigma_l^2 \ge 0, \forall t, \tag{32c}$$

$$\mathbf{W}_{i,l}(t) \succeq 0, \forall t, \tag{32d}$$

$$\text{rank}(\mathbf{W}_{i,l}(t)) = 1, \forall t, \tag{32e}$$

$$(30\text{d}), (30\text{f}). \tag{32f}$$

For notational convenience, we denote the set of $I \times I$ Hermitian positive semidefinite matrices as $\mathfrak{Y} = \{\mathbf{B}|\mathbf{B} \in \mathbb{C}^{I\times I}, \mathbf{B}^T = \mathbf{B}, \mathbf{B} \succeq 0\}$ [31]. Accordingly, (30f) can be written as

$$\mathbf{R}_l(t) \in \mathfrak{Y}. \tag{33}$$

Next, to address the non-concavity of the objective function (32a) and the non-convex constraint (30d), problem (32) remains intractable. To tackle this issue, the fundamental properties of the logarithmic function are used to reformulate the objective function (32a) into (34), as illustrated at the top of next page.

Based on MM algorithm [28], [32], the upper bound of the logarithmic function $\log_2(x)$ is given by

$$\log_2(x) \le \log_2(\tilde{x}) + \frac{1}{\tilde{x}}(x - \tilde{x}), \tag{35}$$

where $\tilde{x}$ is the any given point, and the equality achieved at $x = \tilde{x}$. The upper bound of the concave logarithm function of R_{eve}^1 in (34) can be expressed as

$$R_{\text{eve}}^1 = \log_2\Big(\aleph\big(\mathbf{W}_{k,l}^{(\eta)}(t)\big) + \sum_{l\in\mathcal{L}} \text{Tr}(\mathbf{H}_{e,l}(t)\mathbf{R}_l(t)) + \sigma_e^2\Big)$$
$$+ \frac{\aleph\big(\mathbf{W}_{k,l}(t)\big) - \aleph\big(\mathbf{W}_{k,l}^{(\eta)}(t)\big)}{\aleph\big(\mathbf{W}_{k,l}^{(\eta)}(t)\big) + \sum_{l\in\mathcal{L}} \text{Tr}(\mathbf{H}_{e,l}(t)\mathbf{R}_l(t)) + \sigma_e^2}, \tag{36}$$

where $\mathbf{W}_{k,l}^{\eta}(t)$ is the value of $\mathbf{W}_{k,l}(t)$ at the η-th iteration, and

$$\aleph\big(\mathbf{W}_{k,l(t)}\big) = \sum_{l\in\mathcal{L}} \text{Tr}(\mathbf{H}_{e,l}(t)\mathbf{W}_{k,l}(t))$$
$$+ \sum_{j\in\tilde{\mathcal{K}}\setminus k}\sum_{l\in\mathcal{L}} \text{Tr}(\mathbf{H}_{e,l}(t)\mathbf{W}_{j,l}(t)), \tag{37}$$

$$\aleph\big(\mathbf{W}_{k,l}^{(\eta)}(t)\big) = \sum_{l\in\mathcal{L}} \text{Tr}(\mathbf{H}_{e,l}(t)\mathbf{W}_{k,l}^{(\eta)}(t))$$
$$+ \sum_{j\in\tilde{\mathcal{K}}\setminus k}\sum_{l\in\mathcal{L}} \text{Tr}(\mathbf{H}_{e,l}(t)\mathbf{W}_{j,l}^{(\eta)}(t)). \tag{38}$$

Similarly,

$$R_{\text{leg}}^2 = \log_2\Big(\beth\big(\mathbf{W}_{k,l}^{(\eta)}(t)\big) + \sum_{l\in\mathcal{L}} \text{Tr}(\mathbf{H}_{k,l}(t)\mathbf{R}_l(t)) + \sigma_k^2\Big)$$
$$+ \frac{\beth\big(\mathbf{W}_{k,l}(t)\big) - \beth\big(\mathbf{W}_{k,l}^{(\eta)}(t)\big)}{\beth\big(\mathbf{W}_{k,l}^{(\eta)}(t)\big) + \sum_{l\in\mathcal{L}} \text{Tr}(\mathbf{H}_{k,l}(t)\mathbf{R}_l(t)) + \sigma_k^2}, \tag{39}$$

$$\beth\big(\mathbf{W}_{k,l}(t)\big) = \Big(\sum_{j\in\tilde{\mathcal{K}}\setminus k}\sum_{l\in\mathcal{L}} \text{Tr}(\mathbf{H}_{k,l}(t)\mathbf{W}_{j,l}(t))\Big), \tag{40}$$

$$\beth\big(\mathbf{W}_{k,l}^{(\eta)}(t)\big) = \Big(\sum_{j\in\tilde{\mathcal{K}}\setminus k}\sum_{l\in\mathcal{L}} \text{Tr}(\mathbf{H}_{k,l}(t)\mathbf{W}_{j,l}^{(\eta)}(t))\Big). \tag{41}$$

After substituting the upper bound of R_{eve}^1 from (36) into (34), removing the constant terms in (34), and rank-one terms in (32e), (34) is rewritten as (42) at the top of the next page.

Finally, problem (32) can be convexified as follows:

$$\max_{\substack{\mathbf{w}(t),\\ \mathbf{R}_v(t),\forall t}} \sum_{t\in T}\sum_{k\in\mathcal{K}} \quad \tilde{R}_k^{Sec}(t) \tag{43a}$$

s.t.

$$\tilde{R}_k^{Sec}(t) \ge R_k^{\min}, \quad \forall k,\forall t, \tag{43b}$$

$$(32\text{b}), (32\text{c}), (32\text{d}), (33). \tag{43c}$$

Since problem (43) is convex, it can be solved efficiently by employing convex optimization solvers such as CVX.

B. Phase Shift Optimization

With fixed $\mathbf{w}(t)$, $\mathbf{R}_v(t)$, and $\mathbf{q}(t)$, the subproblem to optimize the URIS reflection vector $\boldsymbol{\theta}(t)$ can be written as

$$\max_{\boldsymbol{\theta}(t),\forall t} \sum_{t\in T}\sum_{k\in\mathcal{K}} \quad [R_k(t) - R_{e,k}(t)] \tag{44a}$$

s.t.

$$(30\text{c}), (30\text{d}), (30\text{e}). \tag{44b}$$

Due to non-convex constraints (30c), (30d), and (30e), it is challenging to design the RIS's phase shifts. In addition, the objective function is a fractional and implicit function of $\boldsymbol{\theta}(t)$, making direct optimization intractable. Let us define $\mathbf{G}_{i,l}(t) = \mathbf{h}_{i,l}(t)\mathbf{h}_{i,l}^H(t)$, $\mathbf{C}_{i,q}(t) = \mathbf{G}_{i,q}(t)\mathbf{w}_{i,l}\mathbf{w}_{i,l}^H\mathbf{G}_{i,q}^H(t)$, $\mathbf{C}_{i,l}(t) = \mathbf{G}_{i,q}(t)\mathbf{R}_l(t)\mathbf{G}_{i,q}^H(t)$, and $\boldsymbol{\psi}(t) = \boldsymbol{\theta}(t)\boldsymbol{\theta}^H(t)$. Then, $R_k(t)$ and $R_{e,k}(t)$ can be rewritten as $\tilde{R}_k(t)$ in (45) and $\tilde{R}_{e,k}(t)$ in (46), respectively, as shown at the top of the next page.

Next, the problem (44) can be reformulated as

$$\max_{\boldsymbol{\psi}(t),\forall t} \sum_{t\in T}\sum_{k\in\mathcal{K}} \quad [\tilde{R}_k(t) - \tilde{R}_{e,k}(t)] \tag{47a}$$

s.t.

$$\hat{\gamma}_s(t) \ge \gamma_s^{\min}, \forall t, \tag{47b}$$

$$(30\text{d}), (30\text{e}), \tag{47c}$$

where $\hat{\gamma}_s(t)$ is given by (48) at the top of the next page.

According to the basic properties of the logarithmic function, the objective function (47a) can be rewritten as (49) at the top of the next page.

$$\hat{R}_k^{\text{Sec}}(t) = \underbrace{\log_2\Big(\sum_{l\in\mathcal{L}}\text{Tr}(\mathbf{H}_{k,l}(t)\mathbf{W}_{k,l}(t)) + \sum_{j\in\tilde{\mathcal{K}}\setminus k}\sum_{l\in\mathcal{L}}\text{Tr}(\mathbf{H}_{k,l}(t)\mathbf{W}_{j,l}(t)) + \sum_{l\in\mathcal{L}}\text{Tr}(\mathbf{H}_{k,l}(t)\mathbf{R}_l(t)) + \sigma_k^2\Big)}_{R_{\text{leg}}^1}$$
$$\underbrace{- \log_2\Big(\sum_{j\in\tilde{\mathcal{K}}\setminus k}\sum_{l\in\mathcal{L}}\text{Tr}(\mathbf{H}_{k,l}(t)\mathbf{W}_{j,l}(t)) + \sum_{l\in\mathcal{L}}\text{Tr}(\mathbf{H}_{k,l}(t)\mathbf{R}_l(t)) + \sigma_k^2\Big)}_{R_{\text{leg}}^2}$$
$$\underbrace{- \log_2\Big(\sum_{l\in\mathcal{L}}\text{Tr}(\mathbf{H}_{e,l}(t)\mathbf{W}_{k,l}(t)) + \sum_{j\in\tilde{\mathcal{K}}\setminus k}\sum_{l\in\mathcal{L}}\text{Tr}(\mathbf{H}_{e,l}(t)\mathbf{W}_{j,l}(t)) + \sum_{l\in\mathcal{L}}\text{Tr}(\mathbf{H}_{e,l}(t)\mathbf{R}_l(t)) + \sigma_e^2\Big)}_{R_{\text{eve}}^1}$$
$$\underbrace{+ \log_2\Big(\sum_{j\in\tilde{\mathcal{K}}\setminus k}\sum_{l\in\mathcal{L}}\text{Tr}(\mathbf{H}_{e,l}(t)\mathbf{W}_{j,l}(t))\sum_{l\in\mathcal{L}}\text{Tr}(\mathbf{H}_{e,l}(t)\mathbf{R}_l(t)) + \sigma_e^2\Big)}_{R_{\text{eve}}^2}, \tag{34}$$

$$\tilde{R}_k^{Sec}(t) = R_{\text{leg}}^1 + R_{\text{eve}}^2 - \frac{\beth\big(\mathbf{W}_{k,l}(t)\big) - \beth\big(\mathbf{W}_{k,l}^{(\eta)}(t)\big)}{\beth\big(\mathbf{W}_{k,l}^{(\eta)}(t)\big) + \sum\limits_{l\in\mathcal{L}}\text{Tr}(\mathbf{H}_{k,l}(t)\mathbf{R}_l(t)) + \sigma_k^2} - \frac{\aleph\big(\mathbf{W}_{k,l}(t)\big) - \aleph\big(\mathbf{W}_{k,l}^{(\eta)}(t)\big)}{\aleph\big(\mathbf{W}_{k,l}^{(\eta)}(t)\big) + \sum\limits_{l\in\mathcal{L}}\text{Tr}(\mathbf{H}_{e,l}(t)\mathbf{R}_l(t)) + \sigma_e^2}, \tag{42}$$

$$\tilde{R}_k(t) = \log_2\left(1 + \frac{\sum\limits_{l\in\mathcal{L}}\Big(\text{Tr}(\mathbf{G}_{k,l}(t)\mathbf{W}_{k,l}(t)) + \text{Tr}(\boldsymbol{\psi}(t)\mathbf{C}_{k,l}(t))\Big)}{\sum\limits_{j\in\tilde{\mathcal{K}}\setminus k}\sum\limits_{l\in\mathcal{L}}\Big(\text{Tr}(\mathbf{G}_{k,l}(t)\mathbf{W}_{j,l}(t)) + \text{Tr}(\boldsymbol{\psi}(t)\mathbf{C}_{k,q}(t))\Big) + \sum\limits_{l\in\mathcal{L}}\Big(\text{Tr}(\mathbf{G}_{e,l}(t)\mathbf{R}_l(t)) + \text{Tr}(\boldsymbol{\psi}(t)\mathbf{C}_{e,q}(t))\Big) + \sigma_k^2}\right), \tag{45}$$

$$\tilde{R}_{e,k}(t) = \log_2\left(1 + \frac{\sum\limits_{l\in\mathcal{L}}\Big(\text{Tr}(\mathbf{G}_{e,l}(t)\mathbf{W}_{k,l}(t)) + \text{Tr}(\boldsymbol{\psi}(t)\mathbf{C}_{e,l}(t))\Big)}{\sum\limits_{j\in\tilde{\mathcal{K}}\setminus k}\sum\limits_{l\in\mathcal{L}}\Big(\text{Tr}(\mathbf{G}_{e,l}(t)\mathbf{W}_{j,l}(t)) + \text{Tr}(\boldsymbol{\psi}(t)\mathbf{C}_{e,q}(t))\Big) + \sum\limits_{l\in\mathcal{L}}\Big(\text{Tr}(\mathbf{G}_{e,l}(t)\mathbf{R}_l(t)) + \text{Tr}(\boldsymbol{\psi}(t)\mathbf{C}_{e,q}(t))\Big) + \sigma_e^2}\right), \tag{46}$$

$$\hat{\gamma}_s(t) = \frac{\sum\limits_{l\in\mathcal{L}}(\sigma_l^l)^2\sum\limits_{k\in\tilde{\mathcal{K}}}\Big(\text{Tr}(\sum\limits_{\acute{l}\in\mathcal{L}}\mathbf{G}_{e,l}(t)\mathbf{W}_{k,l}(t)\mathbf{G}_{e,l}^H(t)) + \text{Tr}(\sum\limits_{\acute{l}\in\mathcal{L}}\boldsymbol{\psi}(t)\mathbf{C}_{e,l}(t)\mathbf{C}_{e,l}^H(t))\Big)}{\sum\limits_{l\in\mathcal{L}}\Big(\text{Tr}(\sum\limits_{\acute{l}\in\mathcal{L}}\mathbf{G}_{e,l}(t)\mathbf{R}_l(t)\mathbf{G}_{e,l}^H(t)) + \text{Tr}(\sum\limits_{\acute{l}\in\mathcal{L}}\boldsymbol{\psi}(t)\mathbf{C}_{e,q}(t)\mathbf{C}_{e,q}^H(t))\Big) + \sigma_e^2}, \tag{48}$$

Based on (35), the upper bound of the concave logarithmic function of $I_2 = I_4 + I_5$ and $I_3 = I_6 + I_7$ in (49) can be respectively expressed as

$$I_2 \le (I_{10} + \sigma_k^2) + \frac{I_1 - I_{10}}{I_{10} + \sigma_k^2}, \tag{50}$$

$$I_3 \le (I_{11} + \sigma_e^2) + \frac{I_{12} - I_{11}}{I_{11} + \sigma_e^2}, \tag{51}$$

where I_{10} and I_{11} are given by (52) and (53) at the top of the next page, respectively. $I_1 = I_4 + I_9$, $I_{12} = I_6 + I_8$, and $\boldsymbol{\psi}^\eta(t)$ is the value of $\boldsymbol{\psi}(t)$ at the η-th iteration. By substituting (50) and (51) into (49) and omitting the constant terms in (49), the problem (47) can be rewritten as

$$\max_{\boldsymbol{\psi}(t),\forall t}\sum_{t\in T}\sum_{k\in\mathcal{K}} \quad (I_{13} + I_{14} + I_{15}) - \frac{I_1 - I_{10}}{I_{10} + \sigma_k^2} - \frac{I_{12} - I_{11}}{I_{11} + \sigma_e^2} \tag{54a}$$

s.t.

$$(I_{13} + I_{14}) - \frac{I_1 - I_{10}}{I_{10} + \sigma_k^2} - \frac{I_{12} - I_{11}}{I_{11} + \sigma_e^2} \ge R_k^{\min}, \tag{54b}$$

$$\hat{\gamma}_s(t) \ge \gamma_s^{\min}, \forall t, \tag{54c}$$

$$\boldsymbol{\psi}(t) \le 1, \forall t. \tag{54d}$$

The problem (54) can be efficiently solved using CVX. If the obtained solution $\boldsymbol{\psi}^\star(t)$ is of rank one, it is regarded as a suboptimal solution. Otherwise, the Gaussian randomization technique is employed to generate the active beamforming

$$
\begin{aligned}
(47a) = \sum_{k\in\mathcal{K}} \Bigg(& \underbrace{\log_2\Bigg(\sum_{l\in\mathcal{L}}\Big(\mathrm{Tr}(\mathbf{G}_{k,l}(t)\mathbf{W}_{k,l}(t))+\mathrm{Tr}(\boldsymbol{\psi}(t)\mathbf{C}_{k,l}(t))\Big)+\sum_{j\in\tilde{\mathcal{K}}\setminus k}\sum_{l\in\mathcal{L}}\Big(\mathrm{Tr}(\mathbf{G}_{k,l}(t)\mathbf{W}_{j,l}(t))+\mathrm{Tr}(\boldsymbol{\psi}(t)\mathbf{C}_{k,q}(t))\Big)}_{I_{13}} \\
& \underbrace{+\sum_{l\in\mathcal{L}}\Big(\mathrm{Tr}(\mathbf{G}_{k,l}(t)\mathbf{R}_l(t))+\mathrm{Tr}(\boldsymbol{\psi}(t)\mathbf{C}_{k,q}(t))\Big)+\sigma_k^2\Bigg)}_{I_{14}} \underbrace{-\log_2\Bigg(\sum_{j\in\tilde{\mathcal{K}}\setminus k}\sum_{l\in\mathcal{L}}\Big(\mathrm{Tr}(\mathbf{G}_{k,l}(t)\mathbf{W}_{j,l}(t))+\mathrm{Tr}(\boldsymbol{\psi}(t)\mathbf{C}_{k,q}(t))\Big)}_{I_4} \\
& \underbrace{\underbrace{+\sum_{l\in\mathcal{L}}\Big(\mathrm{Tr}(\mathbf{G}_{k,l}(t)\mathbf{R}_l(t))+\mathrm{Tr}(\boldsymbol{\psi}(t)\mathbf{C}_{k,q}(t))\Big)}_{I_9}+\sigma_k^2\Bigg)}_{I_5} \underbrace{-\log_2\Bigg(\sum_{l\in\mathcal{L}}\Big(\mathrm{Tr}(\mathbf{G}_{e,l}(t)\mathbf{W}_{k,l}(t))+\mathrm{Tr}(\boldsymbol{\psi}(t)\mathbf{C}_{e,l}(t))\Big)}_{I_6} \\
& \underbrace{+\sum_{j\in\tilde{\mathcal{K}}\setminus k}\sum_{l\in\mathcal{L}}\Big(\mathrm{Tr}(\mathbf{G}_{e,l}(t)\mathbf{W}_{j,l}(t))+\mathrm{Tr}(\boldsymbol{\psi}(t)\mathbf{C}_{e,q}(t))\Big)+\sum_{l\in\mathcal{L}}\Big(\mathrm{Tr}(\mathbf{G}_{e,l}(t)\mathbf{R}_l(t))+\mathrm{Tr}(\boldsymbol{\psi}(t)\mathbf{C}_{e,q}(t))\Big)+\sigma_e^2\Bigg)}_{I_7} \\
& \underbrace{+\log_2\Bigg(\sum_{j\in\tilde{\mathcal{K}}\setminus k}\sum_{l\in\mathcal{L}}\Big(\mathrm{Tr}(\mathbf{G}_{e,l}(t)\mathbf{W}_{j,l}(t))+\mathrm{Tr}(\boldsymbol{\psi}(t)\mathbf{C}_{e,q}(t))\Big)+\sum_{l\in\mathcal{L}}\Big(\mathrm{Tr}(\mathbf{G}_{e,l}(t)\mathbf{R}_l(t))+\mathrm{Tr}(\boldsymbol{\psi}(t)\mathbf{C}_{e,q}(t))\Big)+\sigma_e^2\Bigg)}_{I_{15}}\Bigg), \qquad (49)
\end{aligned}
$$

$$
I_{10}=\log_2\Bigg(\sum_{j\in\tilde{\mathcal{K}}\setminus k}\sum_{l\in\mathcal{L}}\Big(\mathrm{Tr}(\mathbf{G}_{k,l}(t)\mathbf{W}_{j,l}(t))+\mathrm{Tr}(\boldsymbol{\psi}^{\eta}(t)\mathbf{C}_{k,q}(t))\Big)+\sum_{l\in\mathcal{L}}\Big(\mathrm{Tr}(\mathbf{G}_{k,l}(t)\mathbf{R}_l(t))+\mathrm{Tr}(\boldsymbol{\psi}^{\eta}(t)\mathbf{C}_{k,q}(t))\Big)\Bigg), \qquad (52)
$$

$$
\begin{aligned}
I_{11}=\log_2\Bigg(&\sum_{l\in\mathcal{L}}\Big(\mathrm{Tr}(\mathbf{G}_{e,l}(t)\mathbf{W}_{k,l}(t))+\mathrm{Tr}(\boldsymbol{\psi}^{\eta}(t)\mathbf{C}_{e,l}(t))\Big)+\sum_{j\in\tilde{\mathcal{K}}\setminus k}\sum_{l\in\mathcal{L}}\Big(\mathrm{Tr}(\mathbf{G}_{e,l}(t)\mathbf{W}_{j,l}(t))+\mathrm{Tr}(\boldsymbol{\psi}^{\eta}(t)\mathbf{C}_{e,q}(t))\Big)\\
&+\sum_{l\in\mathcal{L}}\Big(\mathrm{Tr}(\mathbf{G}_{e,l}(t)\mathbf{R}_l(t))+\mathrm{Tr}(\boldsymbol{\psi}^{\eta}(t)\mathbf{C}_{e,q}(t))\Big)\Bigg), \qquad (53)
\end{aligned}
$$

vector $\hat{\boldsymbol{\psi}}(t)$.

C. URIS Location Optimization

Before presenting the detailed transformations, we briefly outline the main steps used to solve the URIS trajectory optimization subproblem. The original problem in (55) is non–convex due to the coupled logarithmic terms and the dependence of the channels on the URIS position. First, auxiliary slack variables $\wp(t)$ and $\S(t)$ are introduced to decouple the secrecy rate expression and convert the objective function into a tractable difference form. Then, additional variables $\wp_1(t), \wp_2(t), \mu_k(t), \mu_{k,1}(t), \mu_{k,2}(t), \nu_i(t), \tau_i(t), \natural_{k,i}(t), \rho_{k,i}(t)$ are incorporated to transform the resulting fractional and exponential constraints into equivalent forms. For clarity, the main optimization and slack variables used in this section are summarized in Table II. Finally, SCA and the first–order Taylor expansions are applied to convexify the remaining non–convex terms. After these steps, the subproblem is converted into a standard convex optimization problem that can be efficiently solved using CVX.

TABLE II
SUMMARY OF OPTIMIZATION AND SLACK VARIABLES

Variable	Description
$\mathbf{q}(t)$	URIS 3D position at time slot t
$\wp(t)$	Auxiliary variable for legitimate link rate
$\S(t)$	Auxiliary variable for eavesdropper rate
$\wp_1(t), \wp_2(t)$	Slack variables for UE constraints
$\mu_k(t)$	Slack variable for Eve constraint
$\mu_{k,1}(t), \mu_{k,2}(t)$	Auxiliary exponential variables
$\nu_i(t), \tau_i(t)$	Distance-related slack variables
$\natural_{k,i}(t), \rho_{k,i}(t)$	Linearization variables for SCA

Following are the detailed main steps that are used to optimize the URIS trajectory optimization subproblem. With fixed $\mathbf{w}(t)$, $\mathbf{R}_v(t)$, and $\boldsymbol{\theta}(t)$, the subproblem to optimize the position of URIS $\mathbf{q}(t)$ can be formulated as

$$\max_{\mathbf{q}(t),\forall t} \sum_{t\in T}\sum_{k\in\mathcal{K}} \quad R_k^{\text{Sec}}(t) \tag{55a}$$

s.t.

$$\text{(30c), (30d), (30g), (30h).} \tag{55b}$$

Due to the non-convex nature of the objective function in (55) with respect to $\mathbf{q}(t)$, slack variables $\wp(t)$ and $\S(t)$ are introduced to yield an equivalent and more tractable form of the objective function, which is shown as follows:

$$\max_{\substack{\mathbf{q}(t),\wp(t),\\ \S(t),\forall t}} \sum_{t\in T}\sum_{k\in\mathcal{K}} \quad \Big(\wp(t)-\S(t)\Big) \tag{56a}$$

s.t.

$$e^{\wp(t)} \le \frac{\Pi_{k,1}}{\Pi_{k,2}}, \quad \forall t, \tag{56b}$$

$$e^{\S(t)} \le \frac{\Pi_{e,1}}{\Pi_{e,2}}, \quad \forall t, \tag{56c}$$

$$\text{(30c), (30d), (30g), (30h),} \tag{56d}$$

where $\Pi_{k,1}$, $\Pi_{k,2}$, $\Pi_{e,1}$, and $\Pi_{e,2}$ are given by (57), (58), (59), and (60), respectively, at the top of the next page.

To address the non-convex constraints in (56b) and (56c), we introduce additional slack variables $\wp_1[t]$, $\wp_2[t]$, $\mu_k[t]$, $\mu_{k,1}[t]$, and $\mu_{k,2}[t]$. This transformation enables the reformulation of the problem in (56) into an equivalent form that is easier to optimize, which is given by

$$\max_{\mathcal{V},\forall t} \sum_{t\in T}\sum_{k\in\mathcal{K}} \quad \Big(\wp(t)-\S(t)\Big) \tag{61a}$$

s.t.

$$\wp(t)+\wp_2(t) \le \wp_1(t), \quad \forall t, \tag{61b}$$

$$e^{\S(t)} \le e^{\mu_{k(t)}}, \quad \forall t, \tag{61c}$$

$$\mu_k(t)+\mu_{k,2}(t) \le \mu_{k,1}(t), \quad \forall t, \tag{61d}$$

$$e^{\wp_1(t)} \le \Pi_{k,1}, \quad \forall t, \tag{61e}$$

$$e^{\wp_1(t)} \ge \Pi_{k,2}, \quad \forall t, \tag{61f}$$

$$e^{\mu_{k,1(t)}} \ge \Pi_{e,1}, \quad \forall t, \tag{61g}$$

$$e^{\mu_{k,2(t)}} \le \Pi_{e,2}, \quad \forall t, \tag{61h}$$

$$\text{(30c), (30d), (30g), (30h),} \tag{61i}$$

where

$$\mathcal{V} \triangleq \{\nu[t], t\in\mathcal{T}\},$$
$$\nu[t] = [\mathbf{q}[t], \wp[t], \wp_i[t], \S[t], \mu_k[t], \mu_{k,i}[t]], \forall t, i\in(1,2).$$

Next, the non-convexity of (61) is handled by applying a first-order Taylor expansion to $\S^\eta(t)$ around its value from the the previous iteration. Moreover, the constraints in (61e)–(61h) are convexified by introducing additional slack variables $\nu_i[t]$, $\tau_i[t]$, $\natural_{k,i}[t]$, and $\rho_{k,i}[t]$, with $i\in(1,2)$. Based on these transformations, the problem (61) is reformulated as

$$\max_{\mathbf{Z},\forall t} \sum_{t\in T}\sum_{k\in\mathcal{K}} \quad \Big(\wp(t)-\S(t)\Big) \tag{62a}$$

s.t.

$$\wp(t)+\wp_2(t) \le \wp_1(t), \quad \forall t, \tag{62b}$$

$$e^{\S^\eta(t)} + e^{\S^\eta(t)}\big(\S(t)-\S^\eta(t)\big) \le e^{\mu_{k(t)}}, \quad \forall t, \tag{62c}$$

$$\mu_k(t)+\mu_{k,2}(t) \le \mu_{k,1}(t), \quad \forall t, \tag{62d}$$

$$e^{\wp_1(t)} \le f_1(t), \quad \forall t, \tag{62e}$$

$$e^{\wp_2^\eta(t)} + e^{\wp_2^\eta(t)}\big(\wp_2(t)-\wp_2^\eta(t)\big) \ge f_2(t), \quad \forall t, \tag{62f}$$

$$e^{\mu_{k,1(t)}^\eta} + e^{\mu_{k,1(t)}^\eta}\big(\mu_{k,1(t)}-\mu_{k,1(t)}^\eta\big) \ge f_{e,1}, \quad \forall t, \tag{62g}$$

$$e^{\mu_{k,2(t)}} + \le f_{e,2}(t), \quad \forall t, \tag{62h}$$

$$\nu_1(t) \ge ||\mathbf{q}(t)-\mathbf{p}_k||, \quad \forall t, \tag{62i}$$

$$\tau_1(t) \ge ||\mathbf{q}(t)-\mathbf{p}_l||, \quad \forall t, \tag{62j}$$

$$(\natural_{k,1}(t))^2 \le ||\mathbf{q}^\eta(t)-\mathbf{p}_e||^2 + 2(\mathbf{q}^\eta(t)-\mathbf{p}_e)^T(\mathbf{q}(t)-\mathbf{q}^\eta(t)), \quad \forall t, \tag{62k}$$

$$(\rho_{k,1}(t))^2 \le ||\mathbf{q}^\eta(t)-\mathbf{p}_l||^2 + 2(\mathbf{q}^\eta(t)-\mathbf{p}_l)^T(\mathbf{q}(t)-\mathbf{q}^\eta(t)), \quad \forall t, \tag{62l}$$

$$(\nu_2(t))^2 \le ||\mathbf{q}^\eta(t)-\mathbf{p}_k||^2 + 2(\mathbf{q}^\eta(t)-\mathbf{p}_k)^T(\mathbf{q}(t)-\mathbf{q}^\eta(t)), \quad \forall t, \tag{62m}$$

$$(\tau_2(t))^2 \le ||\mathbf{q}^\eta(t)-\mathbf{p}_l||^2 + 2(\mathbf{q}^\eta(t)-\mathbf{p}_l)^T(\mathbf{q}(t)-\mathbf{q}^\eta(t)), \quad \forall t, \tag{62n}$$

$$\natural_{k,1}(t) \ge ||\mathbf{q}^\eta(t)-\mathbf{p}_e||, \quad \forall t, \tag{62o}$$

$$\rho_{k,1}(t) \ge ||\mathbf{q}^\eta(t)-\mathbf{p}_l||, \quad \forall t, \tag{62p}$$

$$\text{(30c), (30d), (30g), (30h),} \tag{62q}$$

where $\mathbf{Z} \triangleq \{\mathbf{z}(t), t\in T\}$, and $\mathbf{z}(t) = [\nu(t), \nu_i(t), \tau_i(t), \natural_{k,i}(t), \rho_{k,i}(t)]$. In addition, $\wp_i^\eta(t), \mu_i^\eta(t)$, and $\mathbf{q}^\eta(t)$ denote the values obtained in the last iteration. $f_1(t)$ and $f_{e,2}(t)$ are affine functions, $f_2(t)$ and $f_{e,1}(t)$ are convex functions of $\nu_i(t), \tau_i(t), \natural_{k,i}(t), \rho_{k,i}(t)$. The derivations of $f_i(t)$ and $f_{e,i}(t)$ and the associated constraints in (62e)-(62p) are provided in the Appendix. Under these transformations, the URIS trajectory optimization problem in (62) becomes a convex program, which can be efficiently solved using standard convex optimization tools like CVX.

The proposed AO algorithm for addressing problem (30) is outlined in Algorithm 1.

Convergence Analysis: Algorithm 1 is developed based on the AO framework. Let $\{\mathbf{w}^{(\eta)}, \mathbf{R}_v^{(\eta)}, \mathbf{\Theta}^{(\eta)}, \mathbf{q}^{(\eta)}\}$ denote the set of optimization variables at the η-th iteration. The optimization process is carried out as follows: $\cdots \to \big(\mathbf{w}^{(\eta+1)}, \mathbf{R}_v^{(\eta+1)}, \mathbf{\Theta}^{(\eta)}, \mathbf{q}^{(\eta)}\big) \to \big(\mathbf{w}^{(\eta+1)}, \mathbf{R}_v^{(\eta+1)}, \mathbf{\Theta}^{(\eta+1)}, \mathbf{q}^{(\eta)}\big) \to \big(\mathbf{w}^{(\eta+1)}, \mathbf{R}_v^{(\eta+1)}, \mathbf{\Theta}^{(\eta+1)}, \mathbf{q}^{(\eta+1)}\big) \to \ldots$. At each iteration, one block of variables is optimized while keeping the others fixed. First, $\{\mathbf{w}^{(\eta+1)}, \mathbf{R}_v^{(\eta+1)}\}$ are obtained by solving problem (43) with $\{\mathbf{\Theta}^{(\eta)}, \mathbf{q}^{(\eta)}\}$ fixed, which can be expressed as

$$\mathbf{R}_k^{\text{Sec}}\big(\mathbf{w}^{(\eta+1)}, \mathbf{R}_v^{(\eta+1)}, \mathbf{\Theta}^{(\eta)}, \mathbf{q}^{(\eta)}\big) \ge \mathbf{R}_k^{\text{Sec}}\big(\mathbf{w}^{(\eta)}, \mathbf{R}_v^{(\eta)}, \mathbf{\Theta}^{(\eta)}, \mathbf{q}^{(\eta)}\big). \tag{63}$$

Likewise, $\{\mathbf{\Theta}^{(\eta+1)}\}$ is obtained by solving problem (54)

$$\Pi_{k,1} = \log_2\Big(\sum_{l\in\mathcal{L}}\text{Tr}(\mathbf{H}_{k,l}(t)\mathbf{W}_{k,l}(t)) + \sum_{j\in\check{\mathcal{K}}\setminus k}\sum_{l\in\mathcal{L}}\text{Tr}(\mathbf{H}_{k,l}(t)\mathbf{W}_{j,l}(t)) + \sum_{l\in\mathcal{L}}\text{Tr}(\mathbf{H}_{k,l}(t)\mathbf{R}_l(t)) + \sigma_k^2\Big), \tag{57}$$

$$\Pi_{k,2} = \log_2\Big(\sum_{j\in\check{\mathcal{K}}\setminus k}\sum_{l\in\mathcal{L}}\text{Tr}(\mathbf{H}_{k,l}(t)\mathbf{W}_{j,l}(t)) + \sum_{l\in\mathcal{L}}\text{Tr}(\mathbf{H}_{k,l}(t)\mathbf{R}_l(t)) + \sigma_k^2\Big), \tag{58}$$

$$\Pi_{e,1} = \log_2\Big(\sum_{l\in\mathcal{L}}\text{Tr}(\mathbf{H}_{e,l}(t)\mathbf{W}_{k,l}(t)) + \sum_{j\in\check{\mathcal{K}}\setminus k}\sum_{l\in\mathcal{L}}\text{Tr}(\mathbf{H}_{e,l}(t)\mathbf{W}_{j,l}(t)) + \sum_{l\in\mathcal{L}}\text{Tr}(\mathbf{H}_{e,l}(t)\mathbf{R}_l(t)) + \sigma_e^2\Big), \tag{59}$$

$$\Pi_{e,2} = \log_2\Big(\sum_{j\in\check{\mathcal{K}}\setminus k}\sum_{l\in\mathcal{L}}\text{Tr}(\mathbf{H}_{e,l}(t)\mathbf{W}_{j,l}(t))\sum_{l\in\mathcal{L}}\text{Tr}(\mathbf{H}_{e,l}(t)\mathbf{R}_l(t)) + \sigma_e^2\Big), \tag{60}$$

Algorithm 1 Proposed AO Algorithm for Addressing Problem (30)

Initialization: Set $\eta := 0$ and choose an initial feasible point $(\mathbf{w}(t)^0, \mathbf{R}_v(t)^0, \boldsymbol{\theta}(t)^0, \mathbf{q}(t)^0), \forall t$.

1: **repeat**
2: Given $(\boldsymbol{\theta}(t)^\eta, \mathbf{q}(t)^\eta)$, solve convex problem (43) to obtain the optimal $(\mathbf{w}(t)^\star, \mathbf{R}_v(t)^\star)$;
3: Set $(\mathbf{w}(t)^{\eta+1} := \mathbf{w}(t)^\star, \mathbf{R}_v(t)^{\eta+1} := \mathbf{R}_v(t)^\star)$;
4: Given $(\mathbf{w}(t)^{\eta+1}, \mathbf{R}_v(t)^{\eta+1}, \boldsymbol{\theta}(t)^\eta, \mathbf{q}(t)^\eta)$, solve convex problem (54) to obtain the optimal $\boldsymbol{\theta}(t)^\star$;
5: Set $\boldsymbol{\theta}(t)^{\eta+1} := \boldsymbol{\theta}(t)^\star$;
6: Given $(\mathbf{w}(t)^{\eta+1}, \mathbf{R}_v(t)^{\eta+1}, \boldsymbol{\theta}(t)^{\eta+1}, \mathbf{q}(t)^\eta)$, solve convex problem (62) to obtain the optimal $\mathbf{q}(t)^\star$;
7: Set $\mathbf{q}(t)^{\eta+1} := \mathbf{q}(t)^\star$;
8: Set $\eta := \eta + 1$;
9: **until** Convergence criterion is met.
10: **Output**: $(\mathbf{w}(t)^\eta, \mathbf{R}_v(t)^\eta, \boldsymbol{\theta}(t)^\eta, \mathbf{q}(t)^\eta)$.

under fixed $\{\mathbf{w}^{(\eta+1)}, \mathbf{R}_v^{(\eta+1)}, \mathbf{q}^{(\eta)}\}$, which ensures

$$\mathbf{R}_k^{\text{Sec}}\big(\mathbf{w}^{(\eta+1)}, \mathbf{R}_v^{(\eta+1)}, \boldsymbol{\Theta}^{(\eta+1)}, \mathbf{q}^{(\eta)}\big) \geq \mathbf{R}_k^{\text{Sec}}\big(\mathbf{w}^{(\eta+1)}, \mathbf{R}_v^{(\eta+1)}, \boldsymbol{\Theta}^{(\eta)}, \mathbf{q}^{(\eta)}\big). \tag{64}$$

Finally, $\{\mathbf{q}^{(\eta+1)}\}$ is obtained by solving problem (62) with $\{\mathbf{w}^{(\eta+1)}, \mathbf{R}_v^{(\eta+1)}, \boldsymbol{\Theta}^{(\eta+1)}\}$ fixed, yielding

$$\mathbf{R}_k^{\text{Sec}}\big(\mathbf{w}^{(\eta+1)}, \mathbf{R}_v^{(\eta+1)}, \boldsymbol{\Theta}^{(\eta+1)}, \mathbf{q}^{(\eta+1)}\big) \geq \mathbf{R}_k^{\text{Sec}}\big(\mathbf{w}^{(\eta+1)}, \mathbf{R}_v^{(\eta+1)}, \boldsymbol{\Theta}^{(\eta+1)}, \mathbf{q}^{(\eta)}\big). \tag{65}$$

This demonstrates the convergence of the proposed algorithm.

Computational Complexity: In Algorithm 1, all subproblems are solved using the interior-point method. In each iteration, three optimization subproblems are updated sequentially. First, the joint optimization of the transmit beamforming vector $\mathbf{w}$ and AN covariance matrix in (43) involves $LM(K+1)$ beamforming variables and LM AN variables. The convex subproblem solved via SCA requires matrix operations with computational complexity on the order of $\mathcal{O}((LM(K+1))^3 + (LM)^3)$. Second, the URIS phase shift update in (54), solved via SDR combined with SCA, involves N reflecting elements and incurs a computational complexity of $\mathcal{O}(N)^3$. Third, the UAV location update in (62) optimizes $2q$ position variables. The resulting convex optimization subproblem has a computational complexity of $\mathcal{O}((\mathbf{q})^3)$. Therefore, the overall computational complexity per iteration is given by $\mathcal{O}((LM(K+1))^3+(LM)^3+(N)^3+q^3)$.

TABLE III
SIMULATION PARAMETERS

Parameter	Value
Number of APs (L)	4
Antennas per AP (M)	4
Number of LUs (K)	3
Number of RIS elements (N)	10
UAV altitude (H)	50 m
Time slots (T)	10
Carrier frequency	2.7 GHz
Bandwidth	10 MHz
Noise variance (σ_k, σ_e)	-80 dBm [19]
Maximum transmit power ($P_l^{\max}$)	30 dBm
Path-loss at 1 m (J_0)	-20 dB
Path-loss exponent (ground) (α_1)	4.0
Path-loss exponent (air-ground) (α_2)	2.0
Rician factor (κ)	3
Sensing threshold ($\gamma_s^{\min}$)	1 dB [8]
UAV maximum velocity ($v_{\max}$)	20 m/s

V. NUMERICAL RESULTS

In this section, we present simulation results to evaluate the effectiveness of the proposed secure low-altitude URIS-enabled CF-ISAC system. The simulation parameters are summarized in Table III [29], [33]. APs, LUs, and the target/Eve are uniformly distributed within a $100m \times 100m$ square deployment area. All results are obtained in MATLAB using CVX with the SDPT3 solver. The stopping criterion for each AO iteration is based on the relative improvement of the objective function, and the algorithm stops when the increment falls below 10^{-3}.

For performance evaluation, the proposed scheme is evaluated against the following three benchmark schemes:

- **Without AN:** AN is omitted, while the APs' beamformings optimization, RIS's phase shifts optimization, and URIS trajectory design are performed in the same manner as in the proposed scheme.
- **Fixed RIS:** A static RIS is placed at a fixed position, and only the APs' beamformings and RIS's phase shifts are optimized, without using UAV.
- **Without URIS:** A scheme in which only the APs' beamforming vectors are optimized, without employing URIS.

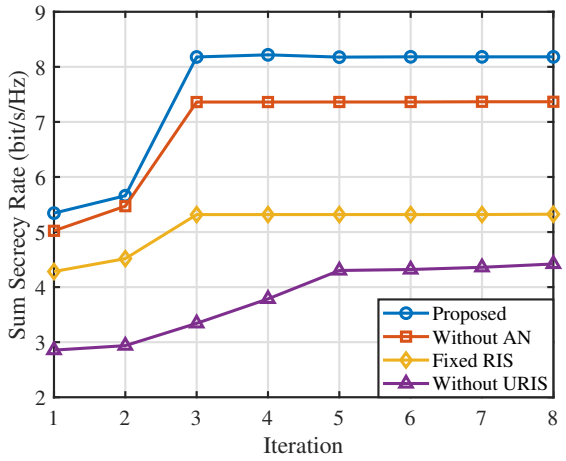

Fig. 2. Convergence behavior of Algorithm 1.

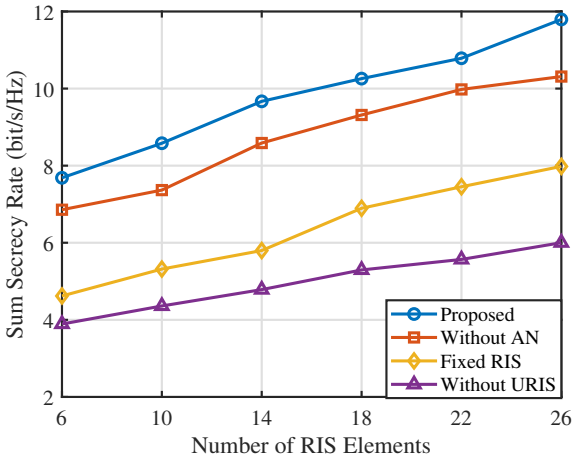

Fig. 3. Impact of the number of RIS elements on the LUs' sum secrecy rate.

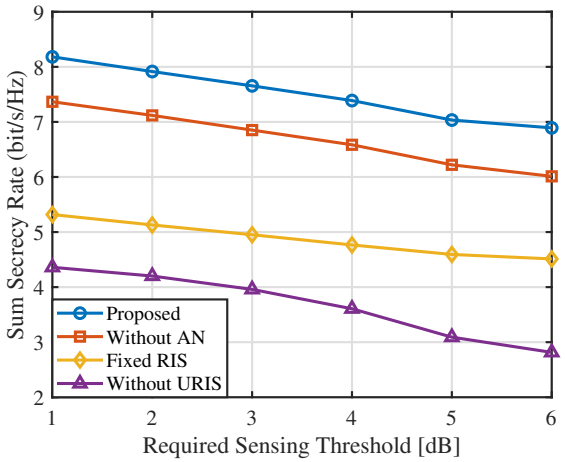

Fig. 4. Impact of sensing threshold requirement on the sum secrecy rate of the LUs.

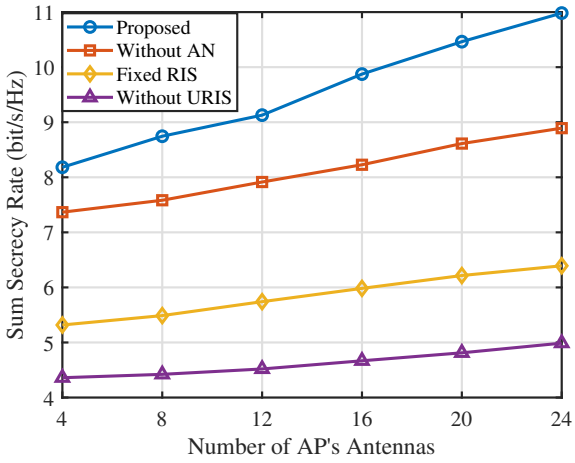

Fig. 5. Impact of number of AP's antennas on the sum secrecy rate.

Fig. 2 depicts the convergence behavior of Algorithm 1. The proposed algorithm converges rapidly and stabilizes within nearly five iterations, confirming the efficiency of the proposed AO algorithm.

The impact of the number of RIS elements on the sum secrecy rate is shown in Fig. 3. We can see that the sum secrecy rate increases as the number of RIS's elements increases. A larger number of RIS's elements offers increased flexibility and greater diversity gain, thus enabling more effective manipulation of the wireless environment. The proposed scheme achieves the best performance at $N = 10$ approximately 16%, 61%, and 96% higher sum secrecy rate compared to the schemes without AN, with fixed RIS, and without URIS, respectively, since deploying UAV and AN adds new degrees of freedom and interference control that help LUs while degrading the Eve's channel. In contrast, schemes without AN or without UAV obtain lower gains, whereas the scheme without using URIS yields the worst performance due to reduced degrees of freedom and no channel enhancement for LUs.

Fig. 4 shows the trade-off between the minimum required sensing threshold and the sum secrecy rate. As the sensing threshold increases, the secrecy performance of all schemes degrades since a higher sensing threshold requires more transmit power to achieve the desired sensing accuracy. Under a fixed total transmit power constraint, allocating more power to sensing reduces the power and degrees of freedom available for AN injection and secrecy-oriented beamforming, which narrows the LUs' SINR advantage over Eve. Consequently, the secrecy rate decreases as the sensing constraint becomes more stringent. In addition, the proposed method demonstrates a considerable secrecy rate advantage over all benchmark schemes, achieving approximately 11%, 54%, and 88% higher sum secrecy rate compared to the schemes without AN, with fixed RIS, and without URIS, respectively, at 1 dB.

Fig. 5 shows the sum secrecy rate versus the number of antennas at each AP. It can be seen that the sum secrecy rate of all schemes improves with the number of AP antennas. It is because a larger antenna array provides higher beamforming gain and additional spatial degrees of freedom, which enhances the desired signal strength at LUs while improving the system's ability to spatially degrade Eve's reception.

VI. Conclusion

This paper investigates a secure ISAC-CF network assisted by a low-altitude URIS. The sum secrecy rate of the consid-

ered network is maximized by jointly optimizing the APs' transmit beamformings, AN, RIS's phase configuration, and the URIS location. As the original problem is non-convex, we decomposed it into three manageable subproblems and developed an iterative AO framework that combines MM, SDR, and SCA methods to efficiently solve them. Simulation results validated the effectiveness of the proposed network compared with benchmarks, and highlighted the potential of deploying low-altitude URIS and AN to provide flexible and robust security enhancements for ISAC-CF networks. Future work may consider multi-UAV coordination, imperfect CSI, and learning-based trajectory optimization to further enhance security and sensing performance.

APPENDIX

This appendix provides the detailed derivations of the expressions for $f_i(t)$ and $f_{e,i}(t)$, together with the convexified constraints given in (62e)–(62p).

To convexify the non-convex constraint (61e), we first rewrite its right-hand side as

$$\Pi_{k,1}(t) \triangleq \Pi_{k,1}^{(a)}(t) + \Pi_{k,1}^{(b)}(t) + \Pi_{k,1}^{(c)}(t) + \sigma_k^2, \tag{66}$$

where the three components of $\Pi_{k,1}(t)$ respectively correspond to: (i) the desired signal power, (ii) multi LU interference, and (iii) AN. The first component $\Pi_{k,1}^{(a)}(t)$ is shown as

$$\begin{aligned}\Pi_{k,1}^{(a)}(t) &\triangleq \sum_{l\in\mathcal{L}} \mathrm{Tr}\big(\mathbf{H}_{k,l}(t)\mathbf{W}_{k,l}(t)\big) \\ &= \sum_{l\in\mathcal{L}} \left(\frac{\mho_1}{d_{l,k}^{\alpha}} + \frac{\mathfrak{E}_1}{d_{l,k}^{\alpha/2} d_{q,k}^{\alpha/2} d_{l,q}^{\alpha/2}} + \frac{\Lambda_1}{d_{q,k}^{\alpha} d_{l,q}^{\alpha}} \right), \end{aligned} \tag{67}$$

where

$$\mho_1 = J_0^2 \sum_{l\in\mathcal{L}} \tilde{\mathbf{h}}_{k,l}^H(t)\mathbf{w}_{k,l}(t)\mathbf{w}_{k,l}^H(t)\tilde{\mathbf{h}}_{k,l}(t),$$

$$\mathfrak{E}_1 = 2J_0 \sum_{l\in\mathcal{L}} \Re\Big\{ \tilde{\mathbf{h}}_{k,l}^H(t)\mathbf{w}_{k,l}(t)\mathbf{w}_{k,l}^H(t)\tilde{\mathbf{h}}_{q,k}^H(t)\mathbf{\Theta}(t)\tilde{\mathbf{H}}_{l,q}(t) \Big\},$$

$$\Lambda_1 = \sum_{l\in\mathcal{L}} \tilde{\mathbf{h}}_{q,k}^H(t)\mathbf{\Theta}(t)\tilde{\mathbf{H}}_{l,q}(t)\mathbf{w}_{k,l}(t)\mathbf{w}_{k,l}^H(t)\tilde{\mathbf{H}}_{l,q}^H(t)\mathbf{\Theta}(t)\tilde{\mathbf{h}}_{q,k}(t).$$

The relevant distances in (67) are defined as $d_{l,k} = \|\mathbf{p}_l - \mathbf{p}_k\|, d_{q,k}(t) = \|\mathbf{q}(t) - \mathbf{p}_k\|, d_{l,q}(t) = \|\mathbf{q}(t) - \mathbf{p}_l\|$, and the corresponding normalized channels are $\mathbf{h}_{l,k} = d_{l,k}^{-\frac{\alpha}{2}}\tilde{\mathbf{h}}_{l,k}, \mathbf{h}_{q,k}(t) = d_{q,k}^{-\frac{\alpha}{2}}\tilde{\mathbf{h}}_{q,k}(t), \mathbf{H}_{l,q}(t) = d_{l,q}^{-\frac{\alpha}{2}}\tilde{\mathbf{H}}_{l,q}(t)$.

Next, the second component $\Pi_{k,1}^{(b)}(t)$ is given by

$$\begin{aligned}\Pi_{k,1}^{(b)}(t) &\triangleq \sum_{j\in\tilde{\mathcal{K}}\setminus\{k\}} \sum_{l\in\mathcal{L}} \mathrm{Tr}\big(\mathbf{H}_{k,l}(t)\mathbf{W}_{j,l}(t)\big) \\ &= \sum_{l\in\mathcal{L}} \left(\frac{\mho_2}{d_{l,k}^{\alpha}} + \frac{\mathfrak{E}_2}{d_{l,k}^{\alpha/2} d_{q,k}^{\alpha/2} d_{l,q}^{\alpha/2}} + \frac{\Lambda_2}{d_{q,k}^{\alpha} d_{l,q}^{\alpha}} \right), \end{aligned} \tag{68}$$

where $\mho_2$, $\mathfrak{E}_2$, and Λ_2 are defined analogously to $\mho_1$, $\mathfrak{E}_1$, and Λ_1, but using $\mathbf{W}_{j,l}(t)$ for $j \neq k$.

Then, the third component $\Pi_{k,1}^{(c)}(t)$ is written as

$$\begin{aligned}\Pi_{k,1}^{(c)}(t) &\triangleq \sum_{l\in\mathcal{L}} \mathrm{Tr}\big(\mathbf{H}_{k,l}(t)\mathbf{R}_l(t)\big) \\ &= \sum_{l\in\mathcal{L}} \left(\frac{\mho_3}{d_{l,k}^{\alpha}} + \frac{\mathfrak{E}_3}{d_{l,k}^{\alpha/2} d_{q,k}^{\alpha/2} d_{l,q}^{\alpha/2}} + \frac{\Lambda_3}{d_{q,k}^{\alpha} d_{l,q}^{\alpha}} \right), \end{aligned} \tag{69}$$

where

$$\mho_3 = J_0^2 \sum_{l\in\mathcal{L}} \tilde{\mathbf{h}}_{k,l}^H(t)\mathbf{v}_l(t)\mathbf{v}_l^H(t)\tilde{\mathbf{h}}_{k,l}(t),$$

$$\mathfrak{E}_3 = 2J_0 \sum_{l\in\mathcal{L}} \Re\Big\{ \tilde{\mathbf{h}}_{k,l}^H(t)\mathbf{v}_l(t)\mathbf{v}_l^H(t)\tilde{\mathbf{h}}_{q,k}^H(t)\mathbf{\Theta}(t)\tilde{\mathbf{H}}_{l,q}(t) \Big\},$$

$$\Lambda_3 = \sum_{l\in\mathcal{L}} \tilde{\mathbf{h}}_{q,k}^H(t)\mathbf{\Theta}(t)\tilde{\mathbf{H}}_{l,q}(t)\mathbf{v}_l(t)\mathbf{v}_l^H(t)\tilde{\mathbf{H}}_{l,q}^H(t)\mathbf{\Theta}(t)\tilde{\mathbf{h}}_{q,k}(t).$$

To convexify the constraint (62e), we introduce the following slack variables $\nu_1(t)$, $\tau_1(t)$, $\nu_2(t)$, and $\tau_2(t)$:

$$\nu_1(t) \geq \|\mathbf{q}(t) - \mathbf{p}_k\|, \quad \tau_1(t) \geq \|\mathbf{q}(t) - \mathbf{p}_l\|, \quad \forall t, \tag{70}$$

$$\nu_2(t) \leq \|\mathbf{q}(t) - \mathbf{p}_k\|, \quad \tau_2(t) \leq \|\mathbf{q}(t) - \mathbf{p}_l\|, \quad \forall t. \tag{71}$$

Let us define

$$\delta_1(t) = \begin{cases} \nu_1(t)\tau_1(t), & \Lambda > 0, \\ \nu_2(t)\tau_2(t), & \Lambda < 0. \end{cases} \tag{72}$$

The non-convex parts in (71) are linearized by the first-order Taylor expansion around the previous URIS location $\mathbf{q}^{\eta}(t)$:

$$(\nu_2(t))^2 \leq \|\mathbf{q}^{\eta}(t) - \mathbf{p}_k\|^2 + 2(\mathbf{q}^{\eta}(t) - \mathbf{p}_k)^{\top}(\mathbf{q}(t) - \mathbf{q}^{\eta}(t)), \tag{73}$$

$$(\tau_2(t))^2 \leq \|\mathbf{q}^{\eta}(t) - \mathbf{p}_l\|^2 + 2(\mathbf{q}^{\eta}(t) - \mathbf{p}_l)^{\top}(\mathbf{q}(t) - \mathbf{q}^{\eta}(t)). \tag{74}$$

By substituting these convex approximations into (62e), it yields

$$e^{\wp_1(t)} \leq f_1(t), \quad \forall t, \tag{75}$$

where

$$f_1(t) = \begin{cases} \mho + \mathfrak{E}\,\chi_1 + \Lambda\,\chi_1 + \sigma_k^2, & \Lambda > 0, \\ \mho + \mathfrak{E}\,\chi_2 + \Lambda\,\chi_2 + \sigma_k^2, & \Lambda < 0, \end{cases} \tag{76}$$

and the linearized coefficients are

$$\chi_1 = \frac{1}{\nu_1^{\eta}(t)\tau_1^{\eta}(t)} - \frac{\nu_1(t) - \nu_1^{\eta}(t)}{(\nu_1^{\eta}(t))^2\tau_1^{\eta}(t)} - \frac{\tau_1(t) - \tau_1^{\eta}(t)}{\nu_1^{\eta}(t)(\tau_1^{\eta}(t))^2}, \tag{77}$$

$$\chi_2 = \frac{1}{\nu_2^{\eta}(t)\tau_2^{\eta}(t)} - \frac{\nu_2(t) - \nu_2^{\eta}(t)}{(\nu_2^{\eta}(t))^2\tau_2^{\eta}(t)} - \frac{\tau_2(t) - \tau_2^{\eta}(t)}{\nu_2^{\eta}(t)(\tau_2^{\eta}(t))^2}. \tag{78}$$

Because $f_1(t)$ is affine when $\Lambda > 0$ and concave when $\Lambda < 0$, the constraint becomes convex in both cases. By substituting the convex approximations of the distance-dependent terms into (62f), it yields

$$e^{\wp_2(t)} \geq f_2(t), \quad \forall t, \tag{79}$$

where $f_2(t)$ is the convex surrogate of $\Pi_{k,1}^{(b)}(t) + \Pi_{k,1}^{(c)}(t) + \sigma_k^2$.

Let

$$\tilde{\mho}_2 \triangleq \mho_{2,k} + \mho_{3,k}, \tag{80}$$

$$\tilde{\mathfrak{E}}_2 \triangleq \mathfrak{E}_{2,k} + \mathfrak{E}_{3,k}, \tag{81}$$

$$\tilde{\Lambda}_2 \triangleq \Lambda_{2,k} + \Lambda_{3,k}, \tag{82}$$

denote the combined coefficients of the interference and AN

terms. The associated mixed-distance factor is defined as

$$\delta_2(t) = \begin{cases} \nu_2(t)\,\tau_2(t), & \text{if } \tilde{\Lambda}_2 > 0, \\ \nu_1(t)\,\tau_1(t), & \text{if } \tilde{\Lambda}_2 < 0, \end{cases} \tag{83}$$

which follows the same sign-dependent selection rule as $\delta_1(t)$. Because $f_2(t)$ follows the same first-order Taylor expansion and linearization procedure as $f_1(t)$, its affine form is obtained directly by substituting the corresponding coefficients, which yields

$$f_2(t) = \begin{cases} \tilde{\mho}_2 + \tilde{\mathfrak{E}}_2\,\chi_2(t) + \tilde{\Lambda}_2\,\chi_2(t) + \sigma_k^2, & \tilde{\Lambda}_2 > 0, \\ \tilde{\mho}_2 + \tilde{\mathfrak{E}}_2\,\chi_1(t) + \tilde{\Lambda}_2\,\chi_1(t) + \sigma_k^2, & \tilde{\Lambda}_2 < 0, \end{cases} \tag{84}$$

which is affine in the optimization variables and thus ensures that

$$e^{\wp_2(t)} \geq f_2(t), \tag{85}$$

is a convex constraint.

Similarly, the constraint in (61g) is reformulated into $f_{e,1}(t)$ following the same procedure used for $f_2(t)$. Likewise, the constraint in (61h) is transformed into $f_{e,2}(t)$ in a manner analogous to the derivation of $f_1(t)$, respectively.

The right-hand side of the corresponding constraint for the target/Eve can be decomposed as

$$\Pi_{e,1}(t) \triangleq \Pi_{e,1}^{(a)}(t) + \Pi_{e,1}^{(b)}(t) + \Pi_{e,1}^{(c)}(t) + \sigma_e^2, \tag{86}$$

where the terms respectively represent the desired signal at the target/Eve, the interference from other LUs, and the AN leakage through the URIS. These are defined as

$$\begin{aligned} \Pi_{e,1}^{(a)}(t) &= \sum_{l\in\mathcal{L}} \mathrm{Tr}\big(\mathbf{H}_{e,l}(t)\mathbf{W}_{k,l}(t)\big) \\ &= \sum_{l\in\mathcal{L}} \left(\frac{\mho_{e,1}}{d_{l,e}^{\alpha}} + \frac{\mathfrak{E}_{e,1}}{d_{l,e}^{\alpha/2} d_{q,e}^{\alpha/2} d_{l,q}^{\alpha/2}} + \frac{\Lambda_{e,1}}{d_{q,e}^{\alpha} d_{l,q}^{\alpha}} \right), \end{aligned} \tag{87}$$

where

$$\begin{aligned} \mho_{e,1} &= J_0^2 \sum_{l\in\mathcal{L}} \tilde{\mathbf{h}}_{e,l}^H(t)\mathbf{w}_{k,l}(t)\mathbf{w}_{k,l}^H(t)\tilde{\mathbf{h}}_{e,l}(t), \\ \mathfrak{E}_{e,1} &= 2J_0 \sum_{l\in\mathcal{L}} \Re\Big\{ \tilde{\mathbf{h}}_{e,l}^H(t)\mathbf{w}_{k,l}(t)\mathbf{w}_{k,l}^H(t)\tilde{\mathbf{h}}_{q,e}^H(t)\boldsymbol{\Theta}(t)\tilde{\mathbf{H}}_{l,q}(t) \Big\}, \\ \Lambda_{e,1} &= \sum_{l\in\mathcal{L}} \tilde{\mathbf{h}}_{q,e}^H(t)\boldsymbol{\Theta}(t)\tilde{\mathbf{H}}_{l,q}(t)\mathbf{w}_{k,l}(t)\mathbf{w}_{k,l}^H(t)\tilde{\mathbf{H}}_{l,q}^H(t)\boldsymbol{\Theta}(t)\tilde{\mathbf{h}}_{q,e}(t). \end{aligned}$$

The path distances are similarly defined as $d_{l,e} = \|\mathbf{p}_l - \mathbf{p}_e\|$, $d_{q,e}(t) = \|\mathbf{q}(t) - \mathbf{p}_e\|$, and $d_{l,q}(t) = \|\mathbf{q}(t) - \mathbf{p}_l\|$.

By introducing the same slack variables $\natural_i(t)$ and $\rho_i(t)$ ($i \in \{1,2\}$), the convexified surrogate of the target/Eve's constraint is expressed as

$$f_{e,1}(t) = \begin{cases} \mho_{e,1} + \mathfrak{E}_{e,1}\chi_4(t) + \Lambda_{e,1}\chi_4(t) + \sigma_e^2, & \Lambda_{e,1} > 0, \\ \mho_{e,1} + \mathfrak{E}_{e,1}\chi_3(t) + \Lambda_{e,1}\chi_3(t) + \sigma_e^2, & \Lambda_{e,1} < 0, \end{cases} \tag{88}$$

and $\chi_3(t)$ and $\chi_4(t)$ are defined as

$$\chi_3 = \frac{1}{\natural_1^{\eta}(t)\rho_{k,1}^{\eta}(t)} - \frac{\natural_1(t) - \natural_1^{\eta}(t)}{(\natural_1^{\eta}(t))^2\rho_{k,1}^{\eta}(t)} - \frac{\rho_{k,1}(t) - \rho_{k,1}^{\eta}(t)}{\natural_1^{\eta}(t)(\rho_{k,1}^{\eta}(t))^2}, \tag{89}$$

$$\chi_4 = \frac{1}{\natural_2^{\eta}(t)\rho_{k,2}^{\eta}(t)} - \frac{\natural_2(t) - \nu_2^{\eta}(t)}{(\natural_2^{\eta}(t))^2\rho_{k,2}^{\eta}(t)} - \frac{\rho_{k,2}(t) - \rho_{k,2}^{\eta}(t)}{\natural_2^{\eta}(t)(\rho_{k,2}^{\eta}(t))^2}. \tag{90}$$

Similarly, we define $\tilde{\mho}_{e,2} \triangleq \mho_{e,2} + \mho_{e,3}$, $\tilde{\mathfrak{E}}_{e,2} \triangleq \mathfrak{E}_{e,2} + \mathfrak{E}_{e,3}$, $\tilde{\Lambda}_{e,2} \triangleq \Lambda_{e,2} + \Lambda_{e,3}$, where

$$f_{e,2}(t) = \begin{cases} \tilde{\mho}_{e,2} + \tilde{\mathfrak{E}}_{e,2}\chi_3(t) + \tilde{\Lambda}_{e,2}\chi_3(t) + \sigma_e^2, & \tilde{\Lambda}_{e,2} > 0, \\ \tilde{\mho}_{e,2} + \tilde{\mathfrak{E}}_{e,2}\chi_4(t) + \tilde{\Lambda}_{e,2}\chi_4(t) + \sigma_e^2, & \tilde{\Lambda}_{e,2} < 0. \end{cases} \tag{91}$$

Both $f_{e,1}(t)$ and $f_{e,2}(t)$ are affine in the optimization variables and hence preserve convexity under the SCA framework, where $\natural_{k,i}(t)$ and $\rho_{k,i}(t), i \in (1,2)$, denote the values obtained from the previous iteration, and the constraints associated with these slack variables can be formulated as follows:

$$\begin{aligned} &(\natural_{k,1}(t))^2 \leq \|\mathbf{q}^{\eta}(t) - \mathbf{p}_e\|^2 \\ &\qquad + 2(\mathbf{q}^{\eta}(t) - \mathbf{p}_e)^T(\mathbf{q}(t) - \mathbf{q}^{\eta}(t)), \quad \forall t, \\ &(\rho_{k,1}(t))^2 \leq \|\mathbf{q}^{\eta}(t) - \mathbf{p}_l\|^2 \\ &\qquad + 2(\mathbf{q}^{\eta}(t) - \mathbf{p}_l)^T(\mathbf{q}(t) - \mathbf{q}^{\eta}(t)), \quad \forall t, \\ &\natural_{k,1}(t) \geq \|\mathbf{q}^{\eta}(t) - \mathbf{p}_e\|, \quad \forall t, \\ &\rho_{k,1}(t) \geq \|\mathbf{q}^{\eta}(t) - \mathbf{p}_l\|, \quad \forall t. \end{aligned}$$

REFERENCES

[1] C. G. Brinton *et al.*, "Key focus areas and enabling technologies for 6G," *IEEE Commun. Mag.*, vol. 63, no. 3, pp. 84–91, Mar. 2025.

[2] X. Lin, "The bridge toward 6G: 5G-advanced evolution in 3GPP release I9," *IEEE Commun. Stand. Mag.*, vol. 9, no. 1, pp. 28–35, Mar. 2025.

[3] Z. Wei *et al.*, "Integrated sensing and communication signals toward 5G-A and 6G: A survey," *IEEE Internet Things J.*, vol. 10, no. 13, pp. 11 068–11 092, Jul. 2023.

[4] Z. Liu *et al.*, "Integrated sensing and edge AI: Realizing intelligent perception in 6G," *IEEE Commun. Surv. Tutor.*, pp. 1–1, Jul. 2025.

[5] F. Dong, F. Liu, Y. Cui, W. Wang, K. Han, and Z. Wang, "Sensing as a service in 6G perceptive networks: A unified framework for ISAC resource allocation," *IEEE Trans. Wirel. Commun.*, vol. 22, no. 5, pp. 3522–3536, May 2023.

[6] D. Wen, Y. Zhou, X. Li, Y. Shi, K. Huang, and K. B. Letaief, "A survey on integrated sensing, communication, and computation," *IEEE Commun. Surv. Tutor.*, vol. 27, no. 5, pp. 3058–3098, Oct. 2025.

[7] U. Demirhan and A. Alkhateeb, "Cell-free ISAC MIMO systems: Joint sensing and communication beamforming," *IEEE Trans. Commun.*, vol. 73, no. 6, pp. 4454–4468, Jun. 2025.

[8] S. Shakoor, N.-S. Vo, Q. N. Le, B. Canberk, H. Shin, and T. Q. Duong, "Weighted sum rate maximization for RIS-mounted UAV-aided cell-free ISAC systems," *IEEE Trans. Commun.*, vol. 74, pp. 4278–4290, Jan. 2026.

[9] J. Chu, Z. Lu, R. Liu, M. Li, and Q. Liu, "Joint beamforming and reflection design for secure RIS-ISAC systems," *IEEE Trans. Veh. Technol.*, vol. 73, no. 3, pp. 4471–4475, Mar. 2024.

[10] Y. Cao, L. Duan, and R. Zhang, "Sensing for secure communication in ISAC: Protocol design and beamforming optimization," *IEEE Trans. Wirel. Commun.*, vol. 24, no. 2, pp. 1207–1220, Feb. 2025.

[11] J. Zou, C. Masouros, F. Liu, and S. Sun, "Securing the sensing functionality in ISAC networks: An artificial noise design," *IEEE Trans. Veh. Technol.*, vol. 73, no. 11, pp. 17 800–17 805, Nov. 2024.

[12] V. Kumar and M. Chafii, "Beamforming design for secure RIS-enabled ISAC: Passive RIS versus active RIS," *IEEE Trans. Wirel. Commun.*, vol. 24, no. 9, pp. 7719–7732, Sep. 2025.

[13] F. Liu, J. Mu, W. Xu, J. Miao, W. Bazzi, and S. Mumtaz, "Toward secure and energy-efficient ISAC in low-altitude IoT: A game-theoretic DRL framework with adaptive sensing," *IEEE Internet Things J.*, pp. 1–1, Oct. 2025.

[14] S. Shakoor, Q. N. Le, L. D. Nguyen, K. Singh, O. A. Dobre, and T. Q. Duong, "Max-min fairness in active aerial reconfigurable intelligent surface-aided ISAC network," *IEEE Trans. Cogn. Commun. Netw.*, vol. 11, no. 5, pp. 2910–2922, Oct. 2025.

[15] Y. Song *et al.*, "An overview of cellular ISAC for low-altitude UAV: New opportunities and challenges," *IEEE Commun. Mag.*, pp. 1–8, Jul. 2025.

[16] Z. Wu, X. Li, Y. Cai, and W. Yuan, "Joint trajectory and resource allocation design for RIS-assisted UAV-enabled ISAC systems," *IEEE Wirel. Commun. Lett.*, vol. 13, no. 5, pp. 1384–1388, May 2024.

[17] S. Shakoor, Z. Kaleem, D.-T. Do, O. A. Dobre, and A. Jamalipour, "Joint optimization of UAV 3-D placement and path-loss factor for energy-efficient maximal coverage," *IEEE Internet Things J.*, vol. 8, no. 12, pp. 9776–9786, Jun. 2021.

[18] R. Liu, M. Li, Q. Liu, and A. L. Swindlehurst, "SNR/CRB-constrained joint beamforming and reflection designs for RIS-ISAC systems," *IEEE Trans. Wirel. Commun.*, vol. 23, no. 7, pp. 7456–7470, Jul. 2024.

[19] Y. Wen, G. Chen, S. Fang, M. Wen, S. Tomasin, and M. Di Renzo, "RIS-assisted UAV secure communications with artificial noise-aware trajectory design against multiple colluding curious users," *IEEE Trans. Inf. Forensics Secur.*, vol. 19, pp. 3064–3076, Jan. 2024.

[20] N. Su, F. Liu, and C. Masouros, "Sensing-assisted eavesdropper estimation: An ISAC breakthrough in physical layer security," *IEEE Trans. Wirel. Commun.*, vol. 23, no. 4, pp. 3162–3174, Apr. 2024.

[21] R. Yang and H. Du, "Joint precoding and artificial noise design for secure transmission in ISAC system," in *Proc. IEEE 24th Int. Workshop Signal Process. Adv. Wireless Commun. (SPAWC)*, Shanghai, China, Sep. 2023, pp. 16–20.

[22] Y. Liu, M. Jin, Q. Guo, and J. Yao, "Secure beamforming for NOMA-ISAC with system imperfections," *IEEE Commun. Lett.*, vol. 28, no. 7, pp. 1559–1563, Jul. 2024.

[23] Y. S. Atiya, Z. Mobini, H. Q. Ngo, and M. Matthaiou, "Secure transmission in cell-free massive MIMO under active eavesdropping," *IEEE Trans. Wirel. Commun.*, vol. 23, no. 12, pp. 18 036–18 052, Dec. 2024.

[24] S. Shakoor, Q. N. Le, E.-K. Hong, B. Canberk, and T. Q. Duong, "Integrated sensing and communications for reconfigurable intelligent surface-aided cell-free networks," *IEEE Commun. Lett.*, vol. 29, no. 6, pp. 1275–1279, Jun. 2025.

[25] X.-T. Dang, H. V. Nguyen, and O.-S. Shin, "Physical layer security for IRS-UAV-assisted cell-free massive MIMO systems," *IEEE Access*, vol. 12, pp. 89 520–89 537, Jun. 2024.

[26] J. Xing, T. Lv, and Y. Cao, "Secure transmission based on access point classification in cell-free networks," in *Proc. IEEE Globecom Workshops (GC Wkshps)*, Rio de Janeiro, Brazil, Dec. 2022, pp. 1176–1181.

[27] D. Wang *et al.*, "Active aerial reconfigurable intelligent surface assisted secure communications: Integrating sensing and positioning," *IEEE J. Sel. Areas Commun.*, vol. 42, no. 10, pp. 2769–2785, Oct. 2024.

[28] Z. Yang, S. Zhang, G. Chen, Z. Dong, Y. Wu, and D. B. da Costa, "Secure integrated sensing and communication systems assisted by active RIS," *IEEE Trans. Veh. Technol.*, vol. 73, no. 12, pp. 19 791–19 796, Dec 2024.

[29] J. Xu, D. Li, Z. Zhu, Z. Yang, N. Zhao, and D. Niyato, "Anti-jamming design for integrated sensing and communication via Aerial IRS," *IEEE Trans. Commun.*, vol. 72, no. 8, pp. 4607–4619, Aug. 2024.

[30] C. Jiang, C. Zhang, C. Huang, J. Ge, D. Niyato, and C. Yuen, "RIS-assisted ISAC systems for robust secure transmission with imperfect sense estimation," *IEEE Trans. Wirel. Commun.*, vol. 24, no. 5, pp. 3979–3992, May 2025.

[31] N. Su, F. Liu, and C. Masouros, "Secure radar-communication systems with malicious targets: Integrating radar, communications and jamming functionalities," *IEEE Trans. Wirel. Commun.*, vol. 20, no. 1, pp. 83–95, Jan. 2021.

[32] Y. Sun, P. Babu, and D. P. Palomar, "Majorization-minimization algorithms in signal processing, communications, and machine learning," *IEEE Trans. Signal Process.*, vol. 65, no. 3, pp. 794–816, Feb 2017.

[33] X. Chen, X. Cao, L. Xie, and Y. He, "DRL-based joint trajectory planning and beamforming optimization in aerial RIS-assisted ISAC system," in *Proc. IEEE Int. Workshop on Radio Freq. and Antenna Technol. (iWRF&AT)*, Shenzhen, China, Jun. 2024, pp. 510–515.